



Opportunities and challenges of hydrotalcite-related electrocatalysts for seawater splitting: A systematic perspective from materials synthesis, characterization and application

Journal:	<i>Journal of Materials Chemistry A</i>
Manuscript ID	TA-REV-04-2023-002524.R1
Article Type:	Review Article
Date Submitted by the Author:	03-Jul-2023
Complete List of Authors:	Dai, Rongrong; Zhejiang Ocean University Dai, Chenyang; Zhejiang Ocean University Hou, Shujin; Qingdao Institute of BioEnergy and Bioprocess Technology Chinese Academy of Sciences He, Qijun; Zhejiang Ocean University Liu, Baogui; Zhejiang Ocean University Huang, Minghua; Ocean University of China, Jiang, Heqing; Chinese Academy of Sciences, Qingdao Institute of Bioenergy and Bioprocess Technology Li, Mohua; Zhejiang Ocean University Pan, Likun; East China Normal University, Guo, Zheng; Department of Engineering, Aarhus University, Kim, Jeonghun; Yonsei University, Chemical and Biomolecular Engineering Han, Minsu; Yonsei University, Chemical and Biomolecular Engineering; The University of Queensland Australian Institute for Bioengineering and Nanotechnology, Yamauchi, Yusuke; University of Queensland, Chemical Engineering Xu, Xingtao; Zhejiang Ocean University

Opportunities and challenges of hydrotalcite-related electrocatalysts for seawater splitting: A systematic perspective from materials synthesis, characterization and application

Rongrong Dai ^a, Chenyang Dai ^a, Shujin Hou ^{b,*}, Qijun He ^a, Baogui Liu ^c, Minghua Huang ^d, Heqing Jiang ^b, MoHua Li ^a, Likun Pan ^e, Zheng Guo ^f, Jeonghun Kim,^g Minsu Han,^h Yusuke Yamauchi ^{h,i,*}, and Xingtao Xu ^{a,*}

^a School of Ocean Science and Technology, Zhejiang Ocean University, Zhoushan, 316022, China, Email: xingtao.xu@zjou.edu.cn (X. Xu)

^b Laboratory of Functional Membrane Material and Membrane Technology, Qingdao Institute of Bioenergy and Bioprocess Technology, Chinese Academy of Sciences, 266101 Qingdao, P. R. China, Email: housj@qibebt.ac.cn (S. Hou)

^c School of Fishery, Zhejiang Ocean University, Zhoushan 316022, China

^d School of Materials Science and Engineering, Ocean University of China, Qingdao, 266100 China

^e Shanghai Key Laboratory of Magnetic Resonance, School of Physics and Electronic Science, East China Normal University, Shanghai 200062, China

^f Department of Engineering, Aarhus University, Aarhus 8000, Denmark

^g Department of Chemical and Biomolecular Engineering, Yonsei University, 50 Yonsei-ro, Seodaemun-gu, Seoul 03722, South Korea

^h School of Chemical Engineering and Australian Institute for Bioengineering and Nanotechnology (AIBN), The University of Queensland, Brisbane, Queensland 4072, Australia, Email: y.yamauchi@uq.edu.au (Y. Yamauchi)

ⁱ Department of Materials Science and Engineering, School of Engineering, Nagoya University, Furo-cho, Chikusa-ku, Nagoya 464-8601, Japan

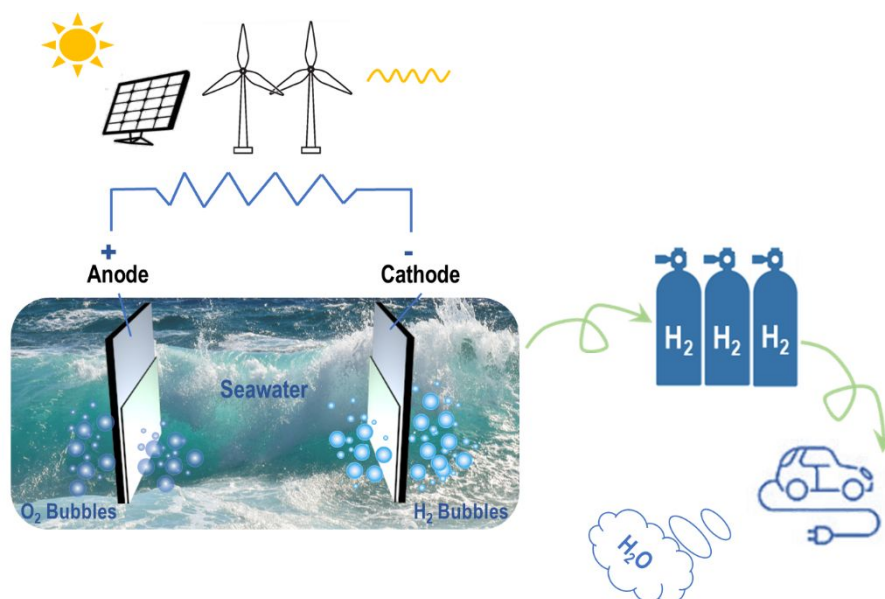
*Corresponding authors.

Abstract

Extensive chloride ions present in seawater can undergo a competitive reaction with water oxidation on the anode during seawater electrocatalysis. The use of alkaline electrolytes enhances the selectivity of seawater oxidation towards the oxygen evolution reaction (OER) rather than the chlorine evolution reaction (CLER) by increasing the potential gap between the two reactions. Layered double hydroxides (LDHs), which can withstand alkaline environments, are suitable for seawater oxidation due to their stability and selectivity. Recent years have witnessed a growing number of publications on LDH-catalyzed seawater splitting. To gain a comprehensive understanding of the current state and challenges of LDH-related electrocatalysts in seawater electrocatalysis, this review conducts a thorough assessment of recent advances in the synthesis, characterization, and electrocatalytic performance of LDH-related materials. Firstly, the review introduces the reaction mechanisms of seawater electrocatalysis over LDH-related materials. The second part presents the common synthetic methods of LDHs, along with the advantages and limitations of each method, as well as various characterization techniques for investigating the structure-activity relationship. Subsequently, the principles for designing LDH-based electrocatalysts and modulating their electrocatalytic activities for seawater splitting are summarized. Furthermore, this review concludes with an analysis of the electrocatalytic performances of LDH derivatives (metal(oxy)hydroxides and phosphides) obtained from LDH precursors. Finally, the challenges and prospects of LDH-related electrocatalysts for seawater electrolysis are discussed.

1. Introduction

The shortage of fossil fuels and environmental pollution caused by burning oil have compelled people to seek cleaner energy sources as alternatives to non-renewable resources. In recent years, hydrogen (H_2) energy has garnered significant attention due to its high energy content of approximately 140 MJ per kg, and the only byproduct of H_2 combustion is water, without any CO_2 emissions.^{1, 2} However, the cleanliness of hydrogen depends on its production method and source.³⁻⁸ Currently, over 85% of H_2 is produced annually from natural gas, coal, and crude oil, resulting in the release of approximately 1 billion tons of CO_2 per year.^{5, 7, 8} Thus, it is crucial to develop greener methods for producing high-purity H_2 . Water splitting, as a technique to produce H_2 , offers environmental friendliness and vast potential. Renewable energy sources such as solar and wind energy, as well as waste heat, can be utilized in water-splitting systems to generate electricity for H_2 production.^{1, 3-5, 7-13} Despite significant research efforts in water electrocatalysis over the past few decades,¹⁴⁻¹⁶ it is important to address the issues associated with the consumption of scarce freshwater as a raw material or the high costs of water purification systems in these studies.^{17, 18}



Scheme 1. Schematic diagram of seawater electrocatalysis.

To address the challenge of high demand for pure water in water splitting, scholars have proposed using seawater as an electrolyte instead of precious freshwater. The schematic diagram in **Scheme 1** illustrates this concept. Direct electrolysis of seawater offers several advantages: i) Seawater accounts for approximately 97% of total water resources, which is around 32 times more abundant than freshwater.^{1, 13, 19} ii) Coastal areas have ample wind and solar energy resources, providing vast renewable energy potential for large-scale electrocatalysis.²⁰⁻²³ iii) Seawater exhibits high ionic conductivity.^{19, 24} iv) When H_2 is converted back to power

through a fuel cell, fresh drinking water is simultaneously produced, making it practical for arid regions.^{1, 25, 26} However, direct seawater electrolysis presents new challenges: i) Seawater contains electrochemically active anions such as Cl^- and Br^- , which can cause anodic reactions during seawater splitting, competing with OER.^{18, 27} ii) Certain metal cations in seawater, such as Ca^{2+} and Mg^{2+} , can form solid precipitates during seawater electrocatalysis, obstructing the active sites of electrocatalysts.^{18, 22, 28, 29} iii) Seawater impurities, including dust and microbes, may adhere to the electrodes and block the active sites of electrocatalysts.^{18, 24, 28, 29} These challenges hinder the industrial implementation of direct seawater electrolysis. However, these issues can be addressed through various methods. For example, solid impurities in seawater can be removed through membranes before seawater electrocatalysis, and the competitive OER reactions can be suppressed by carefully controlling the reaction conditions. Dionigi *et al.* found that alkaline electrolytes can increase the difference between the oxidation potentials of chlorine evolution reaction (CLER) and OER,²⁷ with the largest voltage gap occurring at approximately 480 mV when the solution's pH is higher than 7.5. In other words, alkaline conditions make it possible to achieve 100% seawater oxidation into oxygen on an alkali-tolerant anode catalyst. While some researchers argue that seawater desalination combined with pure water electrolysis is a more promising technology in terms of technological maturity and cost savings,^{6, 20} direct seawater electrolysis, as an emerging technology, offers the significant advantage of not being limited by pure water availability.³⁰ Thus, it is crucial to focus on developing alkali-tolerant electrocatalysts for seawater splitting that exhibit good selectivity and long-term stability.

Solid-based electrocatalysts, characterized by the presence of basic sites on their surfaces and excellent stability in alkaline media, hold great promise for alkaline seawater electrocatalysis. These materials encompass alkaline metal oxides, alkali ion-exchanged/added zeolites, supported alkali materials, clay minerals and so on. Layered double hydroxides (LDHs) belong to the class of anionic clay minerals, represented by the general formula $[\text{M(II)}_{1-x}\text{M(III)}_x(\text{OH})_2]^{x+} \text{A}^{n-}_{x/n} \cdot m\text{H}_2\text{O}$, where M(II) and M(III) denote the metal cations in the LDH layer and A^{n-} represents the interlayer anions. LDHs possess a two-dimensional (2D) structure, as depicted in **Fig. 1a**,³¹ with the partial substitution of M(II) by M(III) resulting in a positive charge within the layer, counterbalanced by A^{n-} . Typically, x falls within the range of 0.2 to 0.4. The abundance of hydroxyl groups in the brucite-like layers of LDHs renders them favorable for operation in alkaline media. The key strengths of LDHs in electrocatalysis include: i) Their low cost and ease of preparation, enabling large-scale production and application. ii) The layer-to-layer structure facilitates exfoliation, yielding ultrathin nanosheets with a large surface area. iii) The compositional flexibility of cations and anions allows

for the tailoring of desired physical and chemical properties. iv) The "memory effect" permits the incorporation of various anions in LDHs. Exploiting these advantages, LDHs have demonstrated versatility in various applications, serving as absorbents,³²⁻³⁵ catalysts,³⁶⁻³⁸ molecular sieves,³⁹ flame retardants,⁴⁰ drug carriers,⁴¹ and more. In addition to these applications, the utilization of LDHs in seawater electrocatalysis represents a promising research area, given their aforementioned characteristics.⁴²⁻⁵⁹ When compared to Pt- and Ru-based catalysts, widely recognized for their excellent electrocatalytic performance,^{2, 60-63} LDH electrocatalysts exhibit distinct advantages, including low cost, ease of preparation, alkaline tolerance, and satisfactory electrocatalytic performance.⁴²⁻⁵⁹

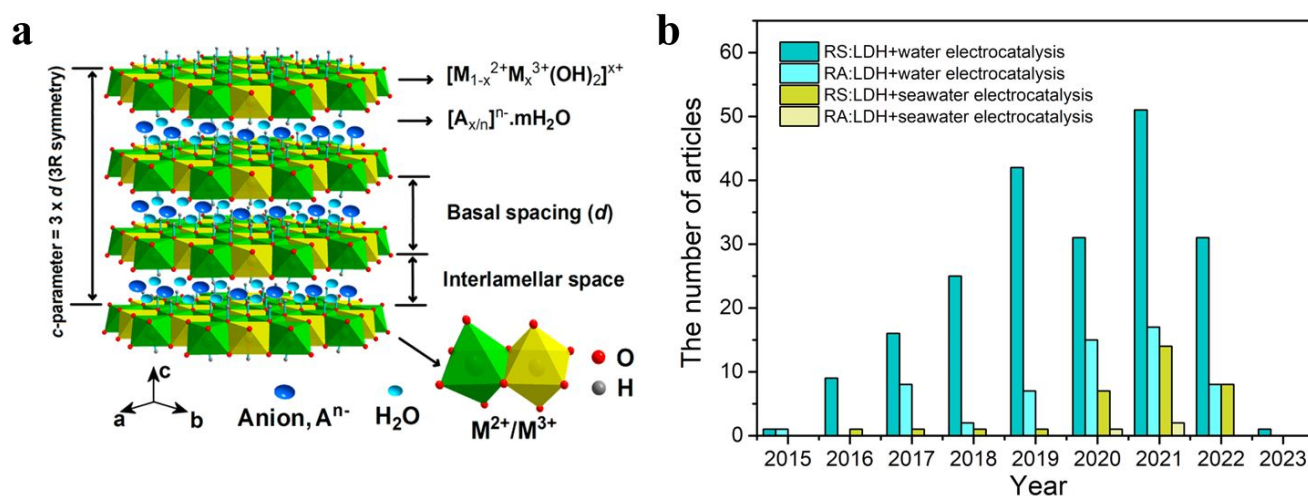


Fig. 1 (a) Classic hydrotalcite structure. Adopted with permission from Li *et al.*³¹ Copyright (2017), MDPI. (b) The number of review and research articles published since 2010; the data was collected from the Web of Science by searching LDH water electrocatalysis or LDH seawater electrocatalysis (Update to October 25, 2022). RS: Research articles; RA: Review articles.

To enhance the electrocatalytic activity of LDH electrocatalysts for seawater electrolysis, researchers have fabricated various LDH composite structures to address limitations such as low active site availability and weak conductivity.^{36, 64} This field of LDHs and LDH-related materials for seawater electrolysis has witnessed a significant surge in research activity in recent years. Therefore, a comprehensive review detailing the current status and challenges of LDHs and LDH-related materials for seawater splitting is imperative to stimulate further research in this domain. **Fig. 1b** provides an overview of the number of published articles focused on water/seawater electrocatalysis using LDHs and LDH-related catalysts in recent years. While numerous reviews on LDHs for water electrocatalysis have been extensively published,^{36, 37} there is a scarcity of systematic reports specifically addressing LDH-related materials in seawater electrocatalysis. This review aims to bridge this gap by presenting the latest advancements in the electrocatalytic mechanisms,

characterization techniques, and catalytic performance of LDH-related materials in seawater electrocatalysis.

2. Mechanism of seawater electrocatalysis over LDHs and simulation calculations

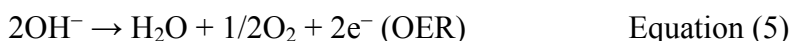
Water/seawater electrocatalysis involves two crucial half-reactions: the hydrogen evolution reaction (HER) and the oxygen evolution reaction (OER).⁸ The specific reaction pathways for HER and OER are determined by the electrolyte conditions in which the electrolysis takes place, as illustrated by the following equations:^{8, 18, 65-67}



For electrolytes with $\text{pH} < 7$ (acidic solution) :



For electrolytes with $\text{pH} \geq 7$ (neutral and alkaline solutions) :

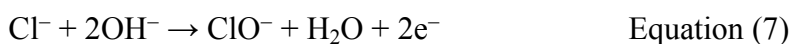


As evident from the above equations, the pathway of water splitting is strongly influenced by the pH of the electrolyte. However, in the case of seawater electrocatalysis, additional challenges arise due to the complex composition of seawater. Liu *et al.* extensively discussed the criteria problem and corresponding solutions for direct seawater electrolysis.⁶⁸ They highlighted that corrosion of electrolytic cells/electrodes and competitive reactions on the anode, such as CLER (Equations 6 and 7), are major obstacles hindering the practical application of direct seawater electrolysis. Consequently, the design of LDH-based electrocatalysts aims to achieve not only higher activity but also excellent resistance to chloride corrosion and selectivity.

In acidic solutions:



In alkaline solutions:



2.1. Mechanism of HER over LDH-related electrocatalysts

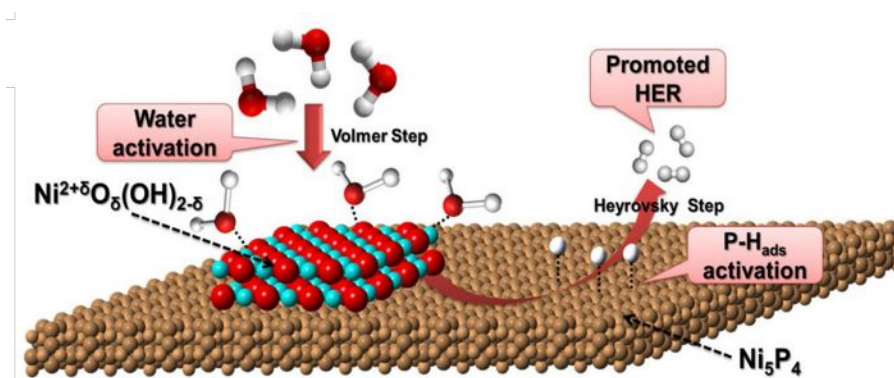


Fig. 2 Schematic diagram of HER by nickel hydr(oxy)oxides electrocatalyst. Reprinted with permission.⁶⁹ Copyright (2019), Elsevier B.V.

In alkaline electrolytes, the HER in seawater splitting involves both Volmer and Heyrovsky kinetic pathways, as illustrated in **Fig. 2**: (1) $*M + H_2O + e^- \rightarrow *MH + OH^-$; (2) $*MH + H_2O + e^- \rightarrow H_2 + OH^-$. Huang *et al.* employed density functional theory (DFT) calculations to investigate nickel hydr(oxy)oxides, Ni_5P_4 nanosheets, and their hybrid composites for HER in seawater electrocatalysis.⁶⁹ The results revealed that the hybrid composites exhibit the lowest free energy for water adsorption compared to nickel hydroxide and Ni_5P_4 nanosheets individually. This favorable water adsorption energy facilitates the initial stage of HER by enhancing water adsorption. Moreover, the optimal Gibbs free energy on the hybrid composite promotes hydrogen adsorption on the surface, thus improving the catalytic HER activity.

2.2. Mechanism of OER over LDH-related electrocatalysts

Fig. 3a illustrates the schematic representation of Ni-Fe oxyhydroxide-catalyzed OER *versus* CLER.⁷⁰ As depicted in **Fig. 3a** and described by Equations (3, 5, 6, and 7), despite OER being thermodynamically more favorable, the kinetic process of OER involves the transfer of four electrons. Consequently, as the potential increases, the kinetically favorable CLER tends to dominate. Dionigi *et al.* conducted experiments to comprehensively analyze the competition between OER and CLER on an anode during seawater electrolysis.²⁷ The calculated Pourbaix diagram from their study is presented in **Fig. 3b**. Their findings suggest that an alkaline electrolyte maximizes the thermodynamic potential difference between CLER and OER, reaching approximately 480 mV at $pH > 7.5$. This condition is conducive to achieving high OER selectivity. The solid-based properties of LDH-based electrocatalysts make them highly suitable for catalytic reactions in alkaline conditions.

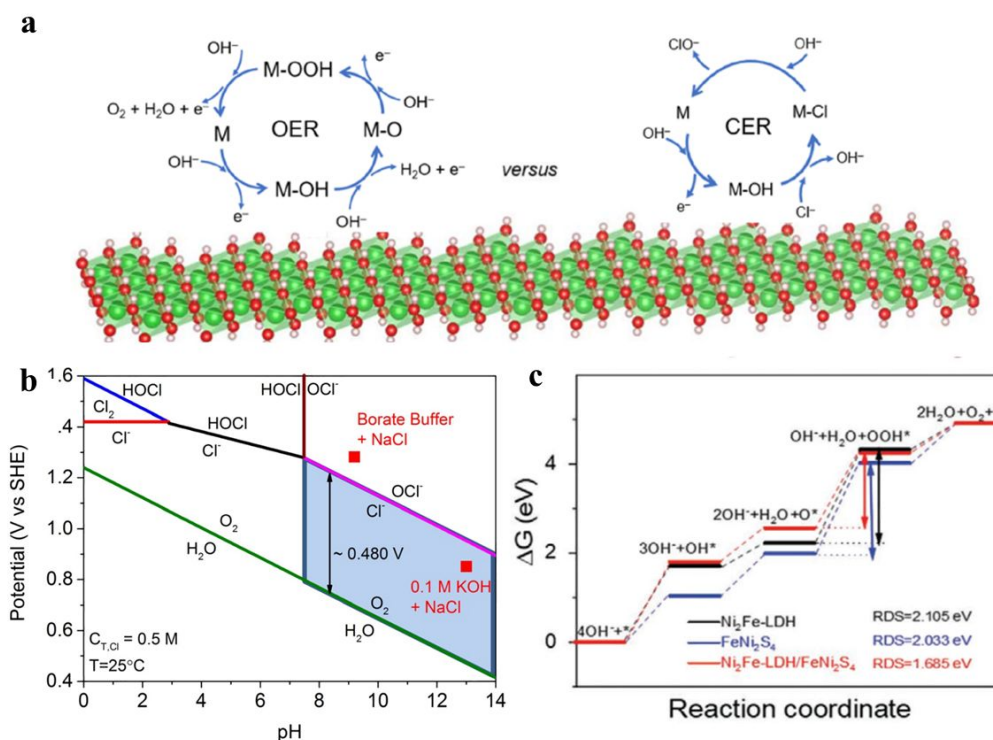


Fig. 3 (a) Schematic diagram of Ni-Fe oxyhydroxide-catalyzed OER vs CLER. Reprinted with permission.⁷⁰ Copyright (2022), American Chemical Society. (b) Pourbaix diagram for the OER and the CLER in saline water. Reprinted with permission.²⁷ Copyright (2016), WILEY-VCH Verlag GmbH & Co. (c) The standard free energy illustration in the OER process on $Ni_2Fe-LDH$, $FeNi_2S_4$, and $Ni_2Fe-LDH/FeNi_2S_4$ at $U = 0$. Reprinted with permission.⁷³ Copyright (2022), Elsevier Ltd.

The OER over LDH-based electrocatalysts in alkaline seawater electrolytes can be investigated through experimental and computational approaches. The inherent electrocatalytic activities of various catalysts for OER can be studied by calculating the standard free energy profiles on the surface models at $U = 0$ V for each reaction step.⁷¹⁻⁷⁴ In the alkaline seawater electrocatalysis, the OER typically involves the following four-step pathways: (1) $*M + OH^- \rightarrow *MOH + e^-$; (2) $*MOH + OH^- \rightarrow H_2O + *MO + e^-$; (3) $*MO + OH^- \rightarrow *MOOH + e^-$ or $2 *MO \rightarrow O_2 + 2 *M$; (4) $*MOOH + OH^- \rightarrow *M + O_2 + e^-$.⁷³

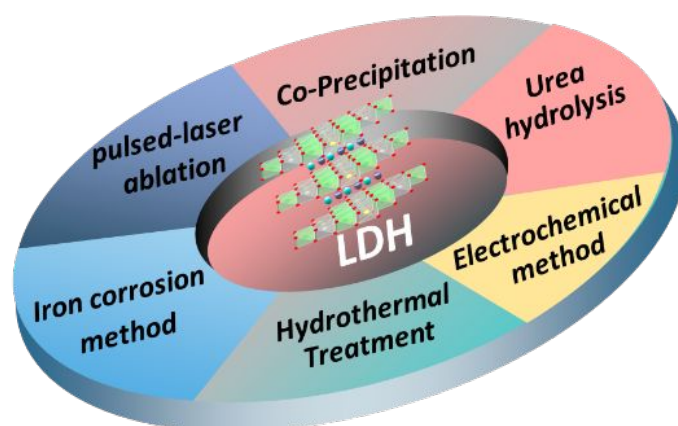
Fig. 3c presents the ΔG diagram of $Ni_2Fe-LDH$, $FeNi_2S_4$, and $Ni_2Fe-LDH/FeNi_2S_4$ based on the calculated results from Tan *et al.*'s work.⁷³ By comparing the ΔG values for each step of the OER process in $Ni_2Fe-LDH$, $FeNi_2S_4$, and $Ni_2Fe-LDH/FeNi_2S_4$, it can be observed that the third step, which involves the generation of the reaction intermediate $*MOOH$, determines the overall reaction rate. Furthermore, $Ni_2Fe-LDH/FeNi_2S_4$ exhibits the lowest total energy barrier ($\Delta G = 1.685$ eV) compared to the other two single-phase electrocatalysts (ΔG of $Ni_2Fe-LDH = 2.105$ eV, ΔG of $FeNi_2S_4 = 2.033$ eV). These DFT calculations provide theoretical evidence that the adsorption and desorption steps of $Ni_2Fe-LDH/FeNi_2S_4$ are optimized compared

to individual single-phase electrocatalysts, resulting in the highest OER activity in alkaline seawater electrolytes.⁷³ In the DFT calculations conducted by You *et al.*,⁷⁴ the rate-determining step for Ni sites in NiFe-LDH and NiIr-LDH is the formation of *MO (step 2), while for Ir sites in NiIr-LDH, it is the formation of the intermediate *MOOH (step 3).

3. Synthesis and Characterization of LDHs

There are several methods available for synthesizing LDHs, as depicted in **Scheme 2**, including co-precipitation, urea hydrolysis, hydrothermal/solvothermal treatment, electrochemical methods, iron corrosion, and pulsed-laser ablation. Among these, co-precipitation and urea hydrolysis are well-established strategies that can be readily scaled up for industrial production. In this section, we provide a comprehensive description of the process and principles behind these various synthetic methods and compare their respective advantages and disadvantages. Additionally, we discuss the advanced characterization techniques employed to investigate LDH-related electrocatalysts.

3.1. The typical synthetic methods of LDHs



Scheme 2. Several synthetic methods of LDHs.

Co-precipitation is a well-established method for synthesizing LDH electrocatalysts.⁷⁴⁻⁷⁶ In the conventional co-precipitation procedure, two solutions are prepared: solution (A) containing the desired amounts of M^{2+} and M^{3+} ions, and solution (B) containing an alkaline precipitant, such as NaOH/ Na_2CO_3 or KOH/ K_2CO_3 . These solutions are simultaneously titrated into distilled water while maintaining a pH of around 8-10 under vigorous stirring. The resulting slurry is then aged at a specific temperature, followed by centrifugation/filtration, washing with distilled water, and drying. Boclair *et al.* provided insights into the crystal formation of LDH,^{77, 78} where aluminum hydroxide or hydrous oxide is formed from Al^{3+} by adjusting the pH of the initial mixture of aqueous solutions. With the addition of alkaline agents, Mg^{2+} cations are

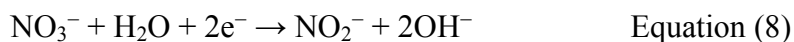
incorporated into the aluminum hydrated oxide, eventually leading to the gradual formation of Mg-Al LDH through the dissolution of $\text{Al}(\text{OH})_3$ in the final stage.^{77, 78} Although the co-precipitation method is simple and convenient to use, the nucleation and growth processes can be challenging to control due to factors such as pH inhomogeneity leading to poor crystallinity and wide size dispersion of crystallites and LDH particles, resulting from varying exposure times for nuclei formed at different stages.⁷⁹

In comparison, urea hydrolysis yields highly crystalline LDH products with a narrow size distribution.^{26, 80} Urea readily dissolves in water and can serve as an alkaline precipitant. The hydrolysis rate of urea can be controlled by adjusting the temperature.⁸¹ Wu *et al.* employed urea hydrolysis in combination with the reduction method to synthesize boron-modified CoFe-LDH.²⁶ In their work, the mole ratio of cobalt ion to ferrum ion in the precursor was found to influence the morphology of the synthesized CoFe-LDHs, with a 2:1 ratio resulting in a hierarchical structure. However, a drawback of urea hydrolysis is its slow nucleation and poor supersaturation during the precipitation process, which can lead to the formation of large LDH particles.^{79, 82}

Another widely used method for synthesizing LDHs is the hydrothermal method.^{45, 55, 57, 73, 83-86} In a typical procedure, a solution containing metal divalent cations, metal trivalent cations, and urea is homogeneously mixed through stirring. The resulting solution is then transferred into an autoclave. Under hydrothermal conditions (*e.g.*, maintaining the autoclave at 120 °C for 12 h), urea decomposes into ammonia, generating OH^- and CO_3^{2-} ions. Subsequently, the metal ions gradually precipitate with OH^- ions, forming a brucite-like layer. Simultaneously, carbonate ions intercalate into the interlayer along with water, resulting in the formation of LDHs. The solvothermal method is similar to the hydrothermal method, with the difference being the introduction of organic solvents, such as N, N-dimethylformamide (DMF), into the synthetic system. This addition of organic solvents leads to the formation of smaller LDH crystals.^{27, 58, 87} Both the hydrothermal and solvothermal methods facilitate the rapid growth of LDH crystals under high pressure, thereby producing highly crystalline LDHs. However, these methods require the use of an autoclave and oven.

To expedite the synthesis of LDHs and reduce costs, researchers continue to explore novel methods. Electrosynthesis is a facile approach for rapidly preparing LDH materials with hierarchical nanostructures.^{46, 51, 52, 88-92} Li *et al.* successfully synthesized ultrathin MFe-LDH nanoplatelet arrays on the surface of Ni foam using electrosynthesis, achieving short reaction times (< 300 s) and low temperatures (room temperature).⁸⁸ They demonstrated that the resulting Ni foam-supported MFe-LDH nanoplatelet arrays could be efficiently synthesized over larger areas, ensuring a consistent surface. Additionally, the Ni foam substrate could be

substituted with other conductive substrates such as conducting carbon cloth and glassy carbon. Li *et al.* highlighted the significance of the reduction process (Equation 8) on the working electrode during electrosynthesis.⁸⁸ This process generates OH⁻ ions, which are then precipitated with M²⁺ and Fe²⁺ ions to form M_xFe_{1-x}(OH)₂ compounds. In the M_xFe_{1-x}(OH)₂ sample, Fe²⁺ undergoes self-oxidation to Fe³⁺, leading to a color change from light green to brownish.



Hydrothermal/solvothermal and electrochemical methods necessitate external energy and specialized equipment for LDH synthesis. In contrast, the iron corrosion method offers a mild condition for producing NiFe LDH.^{93, 94} Liu *et al.* successfully prepared LDH thin films using the iron corrosion method, with a reported thickness of approximately 200 nm, while the LDH nanosheets had a thickness of approximately 8 nm. The resulting LDH materials demonstrated exceptional stability under high current densities. This method is straightforward to execute and can efficiently generate materials over a larger area (0.1 m²).⁹³ The authors proposed a comprehensive formation mechanism for the controlled generation of LDH nanosheet arrays, supported by carefully conducted experiments as depicted in **Fig. 4**. This formation process involves a series of electrochemical reactions (Equations 9-12), driven by the electric potential difference, such as Fe/Fe²⁺ ($\varphi = -0.447$ V) and OH⁻/O₂ ($\varphi = 0.401$ V).⁹³



In the iron corrosion method, the authors highlighted several crucial elements in the synthesis processes: Fe³⁺ and OH⁻ ions, generated through iron corrosion, serve as precursors for LDH nucleation. Divalent metal ions provide the necessary components for LDH growth and create a weakly acidic environment that promotes grain boundary formation in LDH nanosheets. Oxygen is essential for the synthesis as it is required for the corrosion of the iron plate. While carbonate serves as the interlayer balancing anion in LDHs, the presence of carbon dioxide is not significantly important in the corrosion method.⁹³

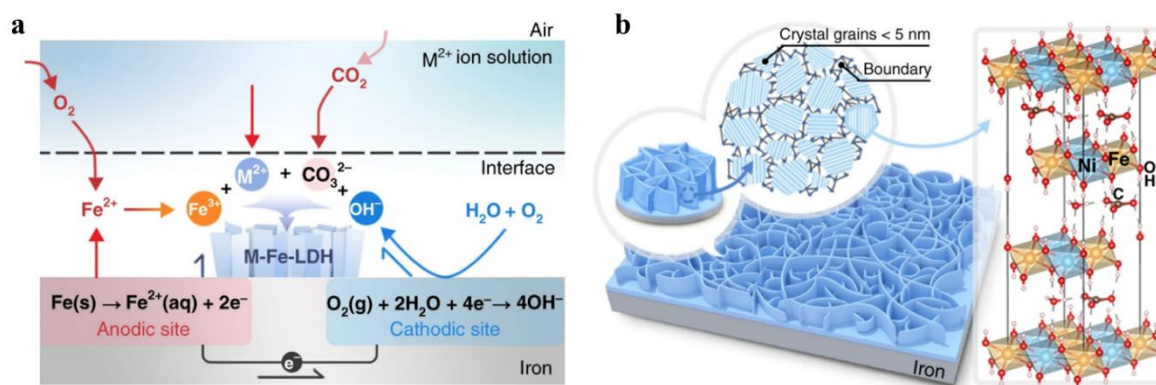


Fig. 4 Schematic diagrams of (a) the production processes and (b) the microstructure of the electrodes. Reprinted with permission.⁹³ Copyright (2018), Nature Publishing Group.

The final synthetic method discussed here is pulsed-laser ablation in liquids (PLAL), which allows for the synthesis of nanomaterials with a narrow size distribution without the need for surfactants. Various parameters in PLAL, such as the type and concentration of metal cations, laser pulse energies, and ablation targets, can be adjusted to kinetically control the particle size and composition of the nanomaterials.^{95, 96} Hunter *et al.* successfully utilized PLAL to prepare a series of nitrate-intercalated NiFe LDHs, and they observed that the electrocatalytic activity improved as the Fe content decreased to 22%.⁹⁶

3.2. The *ex/in-situ* characterization for LDH-based electrocatalysts

Understanding the structural features of catalysts is crucial for uncovering reaction mechanisms and facilitating rational catalyst design. Nuclear magnetic resonance (NMR) spectroscopy is a valuable technique for elucidating the arrangement of metal divalent cations and metal trivalent cations in LDH layers. Sideris *et al.* demonstrated through solid-state NMR analysis that the arrangement of Mg²⁺/Al³⁺ in the layer of MgAl LDH is regular, and there is an absence of Al–O–Al linkages.^{97, 98} Subsequently, Zhao and colleagues further confirmed the non-random distribution of Mg²⁺/Al³⁺ using the "memory effect" of LDH and ¹⁷O NMR spectroscopy.⁹⁹

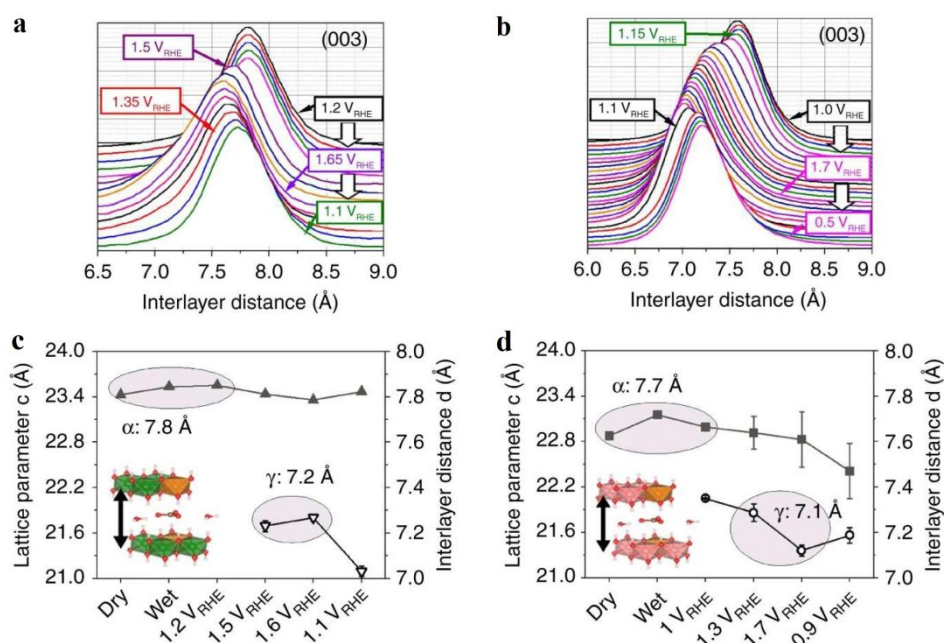


Fig. 5 The waterfall plot and interlayer space for (a, c) NiFe LDH and (b, d) CoFe LDH. Reprinted with permission.⁵⁰ Copyright (2020), Nature Publishing Group.

To investigate the atomic structure of NiFe LDH under catalytic OER conditions, Dionigi *et al.* employed *in-situ* wide-angle X-ray scattering to examine the structural changes of NiFe LDH and CoFe LDH at different oxidation potentials (Fig. 5a, b).⁵⁰ The study revealed that upon reaching a potential higher than the oxidation potential of Ni or Co (approximately 1.6 V), the (003) reflection of the corresponding LDH shifted to a shorter interlayer space, accompanied by the emergence of a shoulder peak at around 7.1 Å (Fig. 5c, d). This newly formed phase was designated as γ-MFe LDH, which was identified as the catalytically active OER phase. Moreover, NiFe LDH displayed a reversible transformation between an initial phase (α-phase) and an activated phase (γ-phase) (Fig. 5a), whereas CoFe LDH exhibited limited reversibility (Fig. 5b).⁵⁰

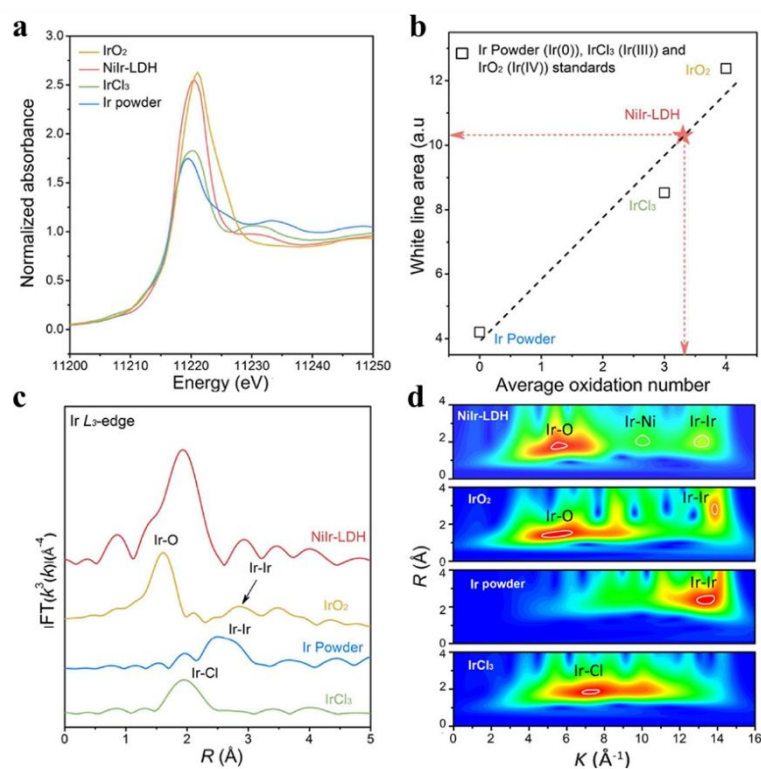


Fig. 6 (a) XANES spectra of Ir L_3 -edge for different catalysts. (b) Calculated Ir oxidation number. (c) Ir EXAFS spectra of L_3 -edge for different catalysts. (d) Ir L_3 -edge wavelet transforms for different Ir signals. Reprinted with permission.⁷⁴ Copyright (2022), American Chemical Society.

The techniques of extended X-ray absorption fine structure (EXAFS) and X-ray absorption near-edge structure (XANES) can detect the chemical environment of cations within the LDH layer, even at low metal site concentrations. In a study conducted by You *et al.*, the electronic structures of LDHs were thoroughly investigated using XANES and EXAFS techniques.⁷⁴ **Fig. 6a** illustrates that the line peak position of NiIr-LDH (red line) falls between those of IrCl_3 (green line) and IrO_2 (yellow line), indicating that the oxidation state of Ir in NiIr-LDH is between that of IrCl_3 and IrO_2 .⁷⁴ Further curve fitting analysis (**Fig. 6b**) revealed an average oxidation number of 3.38 for Ir. The utilization of EXAFS in this study enabled the researchers to elucidate the local coordination environment of the metal atoms.⁷⁴ As depicted in **Fig. 6c**, the primary peak in the NiIr LDH R-space curve appears at 1.9 Å, which lies between the Ir–Cl (2.0 Å) and Ir–O (~1.6 Å) distances. Additionally, a minor shoulder is observed at approximately 2.9 Å, indicating the presence of the overlapping of Ni–Ir and Ir–Ir interactions.⁷⁴ For a more detailed analysis of the local atomic arrangement of Ir, wavelet transforms of the Ir L_3 -edge for different Ir signals were performed (**Fig. 6d**). Comparing the wavelet transforms of NiIr LDH and IrCl_3 , the absence of the Ir–Cl feature in NiIr LDH suggests the lack of Ir–Cl bonds. The wavelet transforms of NiIr LDH exhibit peaks corresponding to the Ir–O and Ir–Ir bonds at

$\sim 1.9 \text{ \AA}$ and $\sim 2.9 \text{ \AA}$, respectively. Based on these findings, the exceptional electrocatalytic activity of NiIr LDH towards OER can be attributed to the reduced electron density of Ni/Ir and the strong interaction between Ni and Ir.⁷⁴

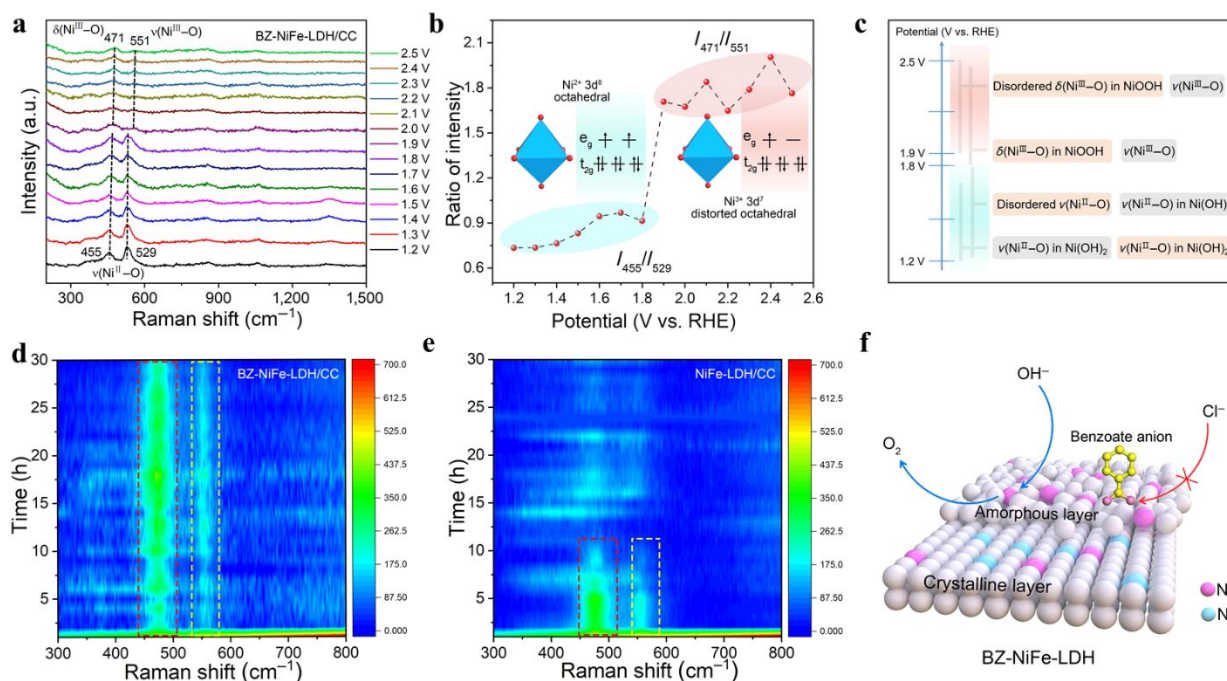


Fig. 7 (a) *Operando* Raman spectra collected for BZ-NiFe-LDH/CC during OER in alkaline seawater. (b) The evolution of I_{455}/I_{529} and I_{471}/I_{551} vs. potential and electronic configuration of Ni^{2+} and Ni^{3+} sites. (c) The light blue region corresponds to the $\nu(\text{Ni}^{\text{II}}-\text{O})$ phase transition of BZ-NiFe-LDH/CC from 1.2 to 1.8 V, while the light pink region shows the $\delta(\text{Ni}^{\text{III}}-\text{O})$ phase transition of BZ-NiFe-LDH/CC from 1.9 to 2.5 V. And *operando* time-dependent Raman spectra collected for (d) BZ-NiFe-LDH/CC and (e) NiFe-LDH/CC electrodes at 1.9 V for 30 h electrolysis in alkaline seawater electrolytes. (f) Schematic picture of OER processes over BZ-NiFe-LDH/CC in alkaline seawater electrolytes. Adopted with permission from Zhang *et al.*,¹⁰⁰ Copyright (2022), SciOpen.

In a recent study by Zhang *et al.*, the *operando* Raman technique was employed to observe the phase evolution of LDH-related electrocatalysts in alkaline seawater.¹⁰⁰ The *operando* Raman spectra of BZ-NiFe-LDH/CC (benzoate anions-intercalated NiFe LDH nanosheet array on carbon cloth) exhibited a redshift trend for the peaks at 455 cm^{-1} and 529 cm^{-1} with increasing applied bias. The decrease in peak densities observed concurrently provided evidence for the formation of $\delta(\text{Ni}^{\text{III}}-\text{O})$ and $(\gamma\text{-NiOOH})$ during the oxidation reaction (Fig. 7a-c).¹⁰⁰ To further characterize the samples, time-dependent *operando* Raman spectra of NiFe LDH and BZ-intercalated NiFe LDH were collected under an applied bias of 1.9 V for 30 h. The authors observed

that the γ -NiOOH peaks remained relatively stable when BZ-NiFe-LDH/CC was immersed in alkaline seawater (0.1 M KOH + seawater) under ongoing oxidation conditions (**Fig. 7d**). In contrast, the γ -NiOOH peaks in the Raman spectra of NiFe-LDH/CC rapidly attenuated within 10 h of operation (**Fig. 7e**), indicating the superior stability of BZ-NiFe-LDH/CC compared to NiFe-LDH/CC, as depicted in **Fig. 7f**.

The remarkable hydrophilic nature of LDH electrocatalysts enhances the adsorption of water molecules during the OER/HER processes, thereby improving mass-transfer efficiency and resulting in an enhanced electrocatalytic activity.⁹⁰ This property can be evaluated through water contact angle measurements.^{90, 101} Jiang *et al.* investigated the hydrophilic/hydrophobic characteristics of NiFe-LDH/FeOOH by measuring the water contact angle.⁹⁰ The observed rapid diffusion of water droplets on the surface of NiFe-LDH/FeOOH (water contact angle $> 90^\circ$) indicated its super hydrophilic nature. This can be attributed to the rapid formation of hydrogen bonds between the water molecules and the OH^- groups present in the NiFe-LDH/FeOOH heterojunction.⁹⁰

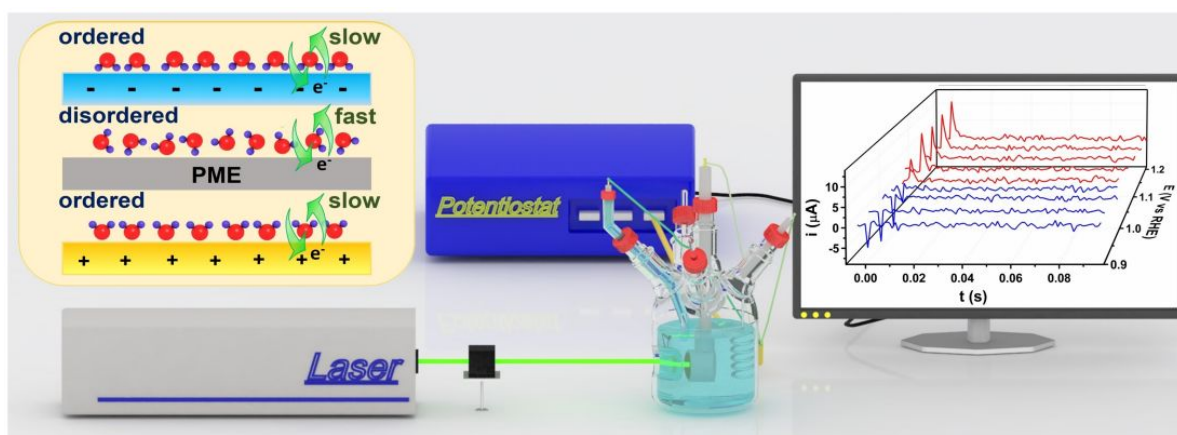


Fig. 8 Schematic picture of the setup of laser-induced current transient which is used to study the interfacial water molecule structure at NiFe(oxy)hydroxide interface. Reprinted with permission.¹⁰³ Copyright (2022), Wiley.

The rigidity or looseness of water molecules at the interface can influence the mobility and interaction of reactants with catalytic active sites. This characteristic is reflected by the potential of maximum entropy (PME).¹⁰² The measurement of PME can be conducted using the laser-induced current transient (LICT) technique.¹⁰³⁻¹⁰⁶ In this technique, as depicted in **Fig. 8**, a pulsed laser beam is directed at the electrode, causing an instantaneous temperature increase that leads to a transition of the water dipole from an ordered to a disordered state within the electric double layer (EDL). Consequently, a sharp current transient is observed due to the rapid relaxation of the disordered state. By studying the laser-induced temperature perturbation, the PME associated with the EDL structure can be determined. Hou *et al.* employed the LICT technique to

investigate the influence of alkali cations in electrolytes on the OER activities of a metal-organic framework (MOF)-derived NiFe (oxy)hydroxide electrocatalyst.¹⁰³ Their findings revealed a correlation between the shift in PME caused by alkali metal cations (Cs^+ , K^+ , Na^+ , Li^+) and the electrocatalytic performance toward OER.

4. Principles for the LDH-based electrocatalysts design and the modulation of electrocatalytic activities

LDH materials have garnered significant attention as effective electrocatalysts for direct seawater electrocatalysis in alkaline electrolytes due to their affordability, thermal stability, earth abundance, and environmental friendliness. The alkaline-tolerant nature, electronic properties, and 2D layered structure of LDH-based electrocatalysts contribute to their immense electrocatalytic potential in seawater. However, challenges such as limited active sites, weak intrinsic activity, and poor electronic conductivity hinder LDHs from achieving higher electrocatalytic efficiency. In this section, we summarize several solutions proposed by researchers to address these issues, as illustrated in **Fig. 9**.

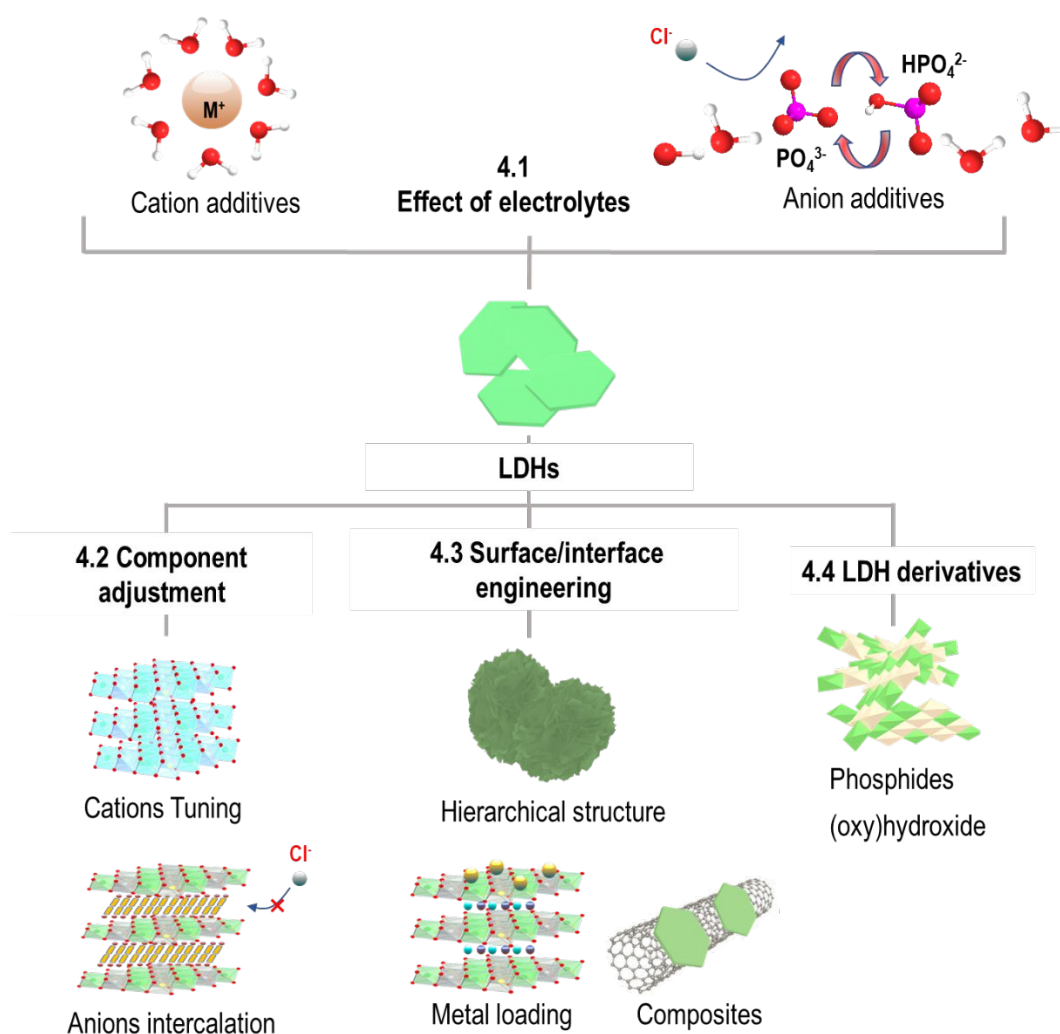


Fig. 9 Schematic diagram of strategies for improving the electrocatalytic activity of LDH-related

electrocatalysts for seawater electrocatalysis.

4.1. The effect of electrolytes for LDH/LDH derivatives on seawater electrolysis

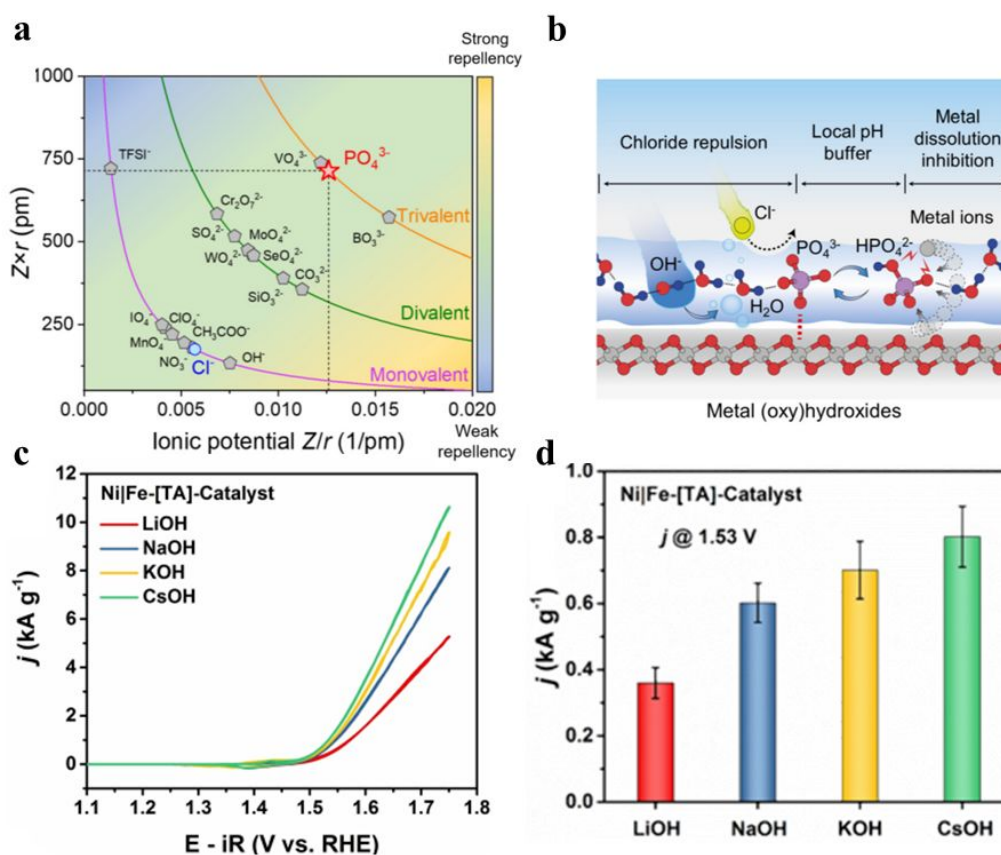


Fig. 10 (a) The ionic potential relationship of common anions and their repulsion to chloride ions; (b) Schematic picture of the surface adsorbed PO_4^{3-} ions protect the catalyst from chloride corrosion. Reprinted with permission.¹⁰⁸ Copyright (2022), Science Press and Dalian Institute of Chemical Physics, Chinese Academy of Sciences. (c) OER polarization curves of SURMOFs-derived electrocatalysts; (d) Comparison of the catalyst mass activities in different alkaline electrolytes. Reprinted with permission.¹⁰³ Copyright (2022), Wiley.

Chloride corrosion poses a challenging issue for anodic current collectors in seawater electrolysis. In the study by Ma *et al.*, it was found that sulfate anions (SO_4^{2-}) present in the electrolytes effectively protect the anodic current collectors against chloride corrosion.¹⁰⁷ Yu *et al.* investigated the impact of anion additives on the OER stability for direct seawater electrocatalysis in alkaline seawater electrolytes, using NiFe-LDH as a representative electrocatalyst.¹⁰⁸ They demonstrated that the presence of PO_4^{3-} ions in the electrolytes significantly enhances the faradaic efficiency and stability of the electrocatalysts. The volcano plot (Fig. 10a) illustrates the balanced relationship of the PO_4^{3-} ion in terms of the value of $Z \times r$ and the ionic potential Z/r ,

compared to other commonly found anions. This indicates the feasibility of stabilizing transition metal ions and preventing chloride adsorption. Additionally, the interaction between the PO_4^{3-} ion and water molecules forms a soft "semipermeable layer" through hydrogen bonding networks, as depicted in **Fig. 10b**. This layer allows easy transport of OH^- ions while effectively inhibiting the movement of Cl^- ions through coulomb repulsion. Furthermore, the transformation of $\text{PO}_4^{3-}/\text{HPO}_4^{2-}$ serves as a buffering mechanism, preventing pH drops under conditions of high current density and thereby improving electrode stability.

The interactions between reactants and hydrated cations at the electrode/electrolyte interface play a crucial role in the electrocatalytic performance of catalysts for OER. Specifically, the presence of alkali metal cations, such as Li^+ , Na^+ , K^+ , and Cs^+ , in the electrolytes can exert an influence on the OER catalytic activity of electrocatalysts.¹⁰⁹ This phenomenon was observed in the study conducted by Hou *et al.*, where it was found that the electrolyte composition has a significant impact on the electrocatalytic performance of the catalysts.¹⁰³ The different alkali metal cations in the electrolytes showed a distinct effect on the OER performances of SURMOF-derived NiFe (oxy)hydroxide, following the order: $\text{Cs}^+ > \text{K}^+ > \text{Na}^+ > \text{Li}^+$ (**Fig. 10c**). Moreover, the SURMOF-derived electrocatalyst exhibited remarkable mass activity in CsOH, surpassing that in KOH, NaOH, and LiOH (**Fig. 10d**). The interaction between the hydroxyl species and the hydrated alkali cations occurs at the electrode/electrolyte interface, where the former is adsorbed while the latter remains in the electrolytes. The strength of this interaction is determined by the hydration energies of alkali metal cations, thereby affecting the OER performance.^{103, 109} For instance, smaller alkali metal cations with larger hydration energies exhibit a stronger interaction with the electrocatalyst, impeding the access of reactants to the active sites of the electrocatalyst.¹⁰³

4.2. Adjustment of LDHs composition

4.2.1. The tuning of layered metal divalent and trivalent cations

The flexible compositions in the brucite-like layer of LDHs, including variations in metal type and metal ratios, contribute to their favorable electronic structure for seawater splitting. **Fig. 11** illustrates the metal cations commonly employed in LDH electrocatalysts for water splitting, as highlighted in purple on the periodic table.^{43, 44, 47-49, 53, 101, 110, 111} Initially, it was discovered that NiFe mixed compounds exhibited remarkable electrocatalytic activity for OER.¹¹²⁻¹¹⁴ Subsequently, crystalline NiFe LDH was successfully synthesized by Gong *et al.* for OER in alkaline media, specifically for freshwater splitting.⁵⁸ Since then, numerous LDH electrocatalysts have been synthesized and developed for catalyzing seawater splitting.^{27, 75,}

80, 94, 115 **Table 1** provides a comprehensive summary of reported LDH electrocatalysts and their performance in OER, both in real and artificial seawater electrolytes.

1												13	14	15	16	17	18	
H	2											B	C	N	O	F	Ne	
Li	Be											Al	Si	P	S	Cl	Ar	
Na	Mg	3	4	5	6	7	8	9	10	11	12	Ga	Ge	As	Se	Br	Kr	
K	Ca	Sc	Ti	V	Cr	Mn	Fe	Co	Ni	Cu	Zn	In	Sn	Sb	Te	I	Xe	
Rb	Sr	Y	Zr	Nb	Mo	Tc	Ru	Rh	Pd	Ag	Cd	Hg	Tl	Pb	Bi	Po	At	Rn
Cs	Ba	La-Lu	Hf	Ta	W	Re	Os	Ir	Pt	Au	Hg	Tl	Pb	Bi	Po	At	Rn	
Fr	Ra	Ac-Lr	Rf	Db	Sg	Bh	Hs	Mt	Rg	Rg	Cn	Uut	Fl	Uup	Lv	Uus	Uuo	

Fig. 11 The reported metal elements used for the preparation of LDH electrocatalysts are marked in purple in the periodic table.

Upon careful analysis of the information presented in **Table 1**, it is evident that Ni-based LDH electrocatalysts^{27, 74, 75, 80, 94, 116} exhibit superior catalytic activity for OER in seawater electrolytes compared to Co-based LDH electrocatalysts.^{92, 111, 117} Notably, Ning *et al.* synthesized a NiFe LDH electrocatalyst using the iron corrosion method,⁹⁴ which demonstrated exceptional stability and catalytic OER activity in an alkaline actual seawater electrolyte (**Table 1**, Entry 3). Furthermore, when combined with NiMoN as a cathode catalyst, the two-electrode electrolyzer (NiFe LDH OER // NiMoN HER) exhibited outstanding activity and durability for electrochemical seawater splitting.⁹⁴ The remarkable seawater oxidation activity of the NiFe LDH can be attributed to its nanosheet array structure and the strongly joint interface between the iron substrate and LDH nanosheet film.⁹⁴ Additionally, beyond the incorporation of 3d transition metals (*e.g.*, Fe), 5d transition metals (*e.g.*, Ir) can also be introduced into Ni-based LDHs for seawater splitting. Cao's group synthesized a novel monolayer NiIr LDH electrocatalyst for seawater electrocatalysis, as shown in **Table 1** (Entry 7), which achieved a large current density (500 mA cm⁻²) at a lower overpotential (361 mV) with approximately 99% O₂ Faradaic efficiency.⁷⁴ The catalytic OER performance of this NiIr LDH electrocatalyst far surpassed that of commercial IrO₂ (763 mV, 23%). Moreover, the NiIr LDH catalyst exhibited remarkable stability, showing only slight activity loss during a longer stability test time (650 h) and at a large current density (500 mA cm⁻²) of an industrial level. According to the authors, the improved electronic structure of the Ni and Ir metal cations in LDH, resulting from their electronic interaction, facilitated electron transfer in the OER processes.⁷⁴ Apart from the metal cation compositions, the ratios of metal divalent cations to metal trivalent cations in the precursor can also alter the nanostructure of NiFe LDH, consequently affecting its OER catalytic activity.⁸⁰ For instance, the controlled incorporation of Fe cations can be employed to modulate the morphology of LDHs,

transforming them from particles into nanosheets. Dong *et al.* reported that a Ni/Fe ratio of 6:4 in the precursor led to the synthesis of a nanosheet-structured NiFe LDH.⁸⁰ This unique morphology contributed to its superior OER activity (**Table 1**, Entry 2) compared to other synthesized NiFe LDH catalysts. Furthermore, the overpotential required by this NiFe LDH to achieve a specific current density was lower than that of the benchmarking RuO₂ catalyst.

According to the Nernst equation, the potential required for OER is significantly influenced by the pH value of the electrolyte. While hydrogen production from neutral or near-neutral media offers cost savings and avoids alkali corrosion, the sluggish kinetics of OER and the poor ionic conductivity in neutral electrolytes hinder the progress of research in this area. Cheng *et al.* synthesized a CoFe LDH electrocatalyst capable of achieving a current density of 10 mA cm⁻² at an overpotential of 530 mV in simulated seawater without the addition of alkaline agents (pH 8).⁷⁶ As observed in **Table 1**, most LDH electrocatalysts employed for seawater oxidation have been tested in alkaline electrolytes, and their catalytic performances generally surpass that of CoFe LDH, which operates in a near-neutral medium.

The brucite-like layer of LDHs offers the opportunity to incorporate more than two types of metal cations, leading to the formation of ternary LDH electrocatalysts and enabling the adjustment of LDHs' electronic structure.^{92, 111} For instance, Liu *et al.* synthesized CoFeZr LDH electrocatalysts with different electrodeposition times and applied them to the seawater splitting reaction.⁹² Through electrochemical responses, XPS spectra, and XRD patterns, they discovered that Zr doping enhanced the electronic structure of CoFe LDH, resulting in the formation of a mixed crystal within CoFe LDH. This modification reduced the adsorption of chloride ions, facilitating a decrease in overpotentials during the OER (**Table 1**, Entry 8) and HER processes.⁹² Additionally, Khatun *et al.* prepared CoCrV LDH by introducing vanadium as a third metal cation into CoCr LDH.¹¹¹ They found that this modification not only introduced additional active sites in the electrocatalyst but also improved electron transfer, thereby enhancing the OER activity and suppressing CLER compared to the original CoCr LDH.

Table 1. The electrocatalytic activities and stabilities for OER in real/simulated seawater electrolytes over different reported LDH electrocatalysts.

Entry	^a OER Electrocatalysts	^b Synthetic method	Electrolytes	η and its corresponding current density	^c Chr Amp	^d Chr Pot	Parameters for service life studies	Refs.
1	NiFe LDH	S	0.5 M NaCl + 1 M KOH	359 mV at 10 mA cm ⁻²	No	Yes	10 mA cm ⁻² @2	27
2	NiFe LDH/CC	U	Actual seawater + 1 M KOH	238 mV at 10 mA cm ⁻² 247 mV at 100 mA cm ⁻²	No	Yes	100 mA cm ⁻² @165	80
3	NiFe LDH/NF	I	Actual seawater + 1 M KOH	296 mV at 500 mA cm ⁻²	No	Yes	500 mA cm ⁻² @96	94

4	NiFe LDH/NF	C	0.5 M NaCl + 1 M KOH	227 mV at 100 mA cm ⁻² ; 257 mV at 500 mA cm ⁻²	No	Yes	100 mA cm ⁻² @ 24 h	75
5	NiFe LDH/NFF	I	0.5 M NaCl + 1 M KOH	178 mV at 100 mA cm ⁻²	-	-	-	116
6	CoFe LDH	C	Simulated seawater	530 mV at 10 mA cm ⁻²	Yes	No	0.56 V@8 h	76
			0.5 M NaCl + 1 M KOH	286 mV at 100 mA cm ⁻²	-	-	-	
7	NiIr-LDH/NF	C	Actual seawater + 1 M KOH	315 mV at 100 mA cm ⁻² ; 361 mV at 500 mA cm ⁻²	No	Yes	500 mA cm ⁻² @ 650 h	74
8	CoFeZr LDH/NF	E	0.5 M NaCl + 1 M KOH	303 mV at 100 mA cm ⁻²	Yes	No	1.66 V@20 h	92
			1 M NaCl + 1 M KOH	300 mV at 10 mA cm ⁻²	-	-	-	
9	CoCrV LDH/NF	H	Actual seawater + 1 M KOH	320 mV at 10 mA cm ⁻²	Yes	No	1.65 V@24 h	111
10	CoNiFe LDH	C	Actual seawater + 1 M KOH	304 mV at 100 mA cm ⁻²	No	Yes	100 mA cm ⁻² @ 80 h	117

^a NF-Ni foam; NFF-NiFe foam; CC-carbon cloth. ^b S-Solvothermal method, UHCR-Urea hydrolysis combined with chemical reduction, HVE-hydrothermal-vulcanization-electrodeposition, C-coprecipitation, E-Electrochemical method, U-Urea hydrolysis, I-iron corrosion method. ^c ChrAmp: Chronoamperometry. ^d ChrPot: Chronopotentiometry.

In conclusion, the composition of metal cations within the LDH electrocatalysts can be adjusted by varying the type and quantity of metal salts used during the synthesis process. This modulation of metal cations, along with the ratio of divalent to trivalent metal cations, influences the intrinsic activity of the synthesized LDH and, consequently, its electrocatalytic performance for OER/HER in alkaline seawater electrolytes. Notably, among LDHs, Ni-based electrocatalysts, particularly NiFe LDH synthesized *via* the iron corrosion method, demonstrate superior performance. Furthermore, the incorporation of a third metal in ternary LDH electrocatalysts can expand the physical interlayer space and enhance the electronic structure of LDHs, resulting in improved activity for seawater splitting.

4.2.2. Regulation of A^n by interlayer intercalation

The interlayer anions present in LDHs serve a dual role: maintaining the layer-to-layer structure as charge-balancing anions and influencing the intrinsic properties of LDHs through their impact on the electron density of metal sites within the layers. Zhou *et al.* observed variations in the catalytic activity of NiFe LDHs for OER in alkaline water after intercalating anions with different redox potentials.¹¹⁸ Remarkably, the OER activity of the LDHs exhibited a linear correlation with the redox potential of the interlayer anions. For instance, fluoride ions, with a high standard redox potential, displayed a weak reducing ability, while hypophosphite exhibited a lower redox potential, indicating a higher reducing ability. Electrochemical measurements revealed that NiFe LDHs intercalated with fluoride ions exhibited superior OER activity compared to those intercalated with hypophosphite.¹¹⁸ Ge *et al.* demonstrated that CoFe LDHs with larger interlayer spacings exhibited enhanced catalytic performance for OER compared to the original CoFe LDH.¹¹⁹ Carrasco *et al.* further

expanded the interlayer space of NiFe LDH electrocatalysts through intercalation of surfactants, resulting in increased electrocatalytic activity for OER.¹²⁰ This phenomenon was also observed by Dong *et al.*, who noted that the intercalation of dicarboxylate anions in NiFe LDHs induced structural instability.¹²¹ This structural distortion led to *in situ* anion exchange during OER catalysis, thereby enhancing the electrocatalytic activity of the catalyst. Additionally, Müller *et al.* reported that the basicity of intercalated anions could impact the electrocatalytic activity of LDHs for OER.¹²²

Similarly, anion intercalation can also influence the electrocatalytic activity of LDHs in seawater oxidation.¹⁰⁰ In the case of BZ-NiFe-LDH/CC, the intercalated benzoate anions (BZ) serve as corrosion inhibitors, protecting against detrimental chlorine (electro)chemistry in seawater electrolytes. They also act as proton acceptors, mitigating pH decrease in the local solution near the LDH electrode. The BZ-NiFe-LDH/CC catalyst exhibits a significant enhancement in OER electrocatalytic activity compared to other catalysts (**Fig. 12a, b**). **Fig. 12c, d** illustrate the overpotentials of 610 mV and 370 mV, respectively, for the BZ-intercalated NiFe LDH catalyst when delivering a large current density (500 mA cm^{-2}) in alkaline actual seawater electrolytes and simulated seawater electrolytes containing NaCl. Furthermore, the BZ-intercalated LDH catalyst demonstrates negligible activity loss at a high current density over an extended period (500 mA cm^{-2} for 100 h).¹⁰⁰ Notably, the stability of BZ-NiFe-LDH/CC surpasses that of non-BZ-intercalated NiFe-LDH/CC catalyst in alkaline seawater electrolytes.¹⁰⁰ Analysis of metal cation leaching from the catalysts in seawater electrolytes after electrolysis using ICP-OES reveals that nickel ions are more prone to leaching from NiFe-LDH/CC compared to BZ-intercalated NiFe-LDH/CC. This promotion is attributed to the ability of BZ anions to impede LDH dissolution by hindering the diffusion of chloride ions, while simultaneously enlarging the interlayer spacing to facilitate electrolyte penetration and diffusion in the catalyst (**Fig. 12e, f**).¹⁰⁰

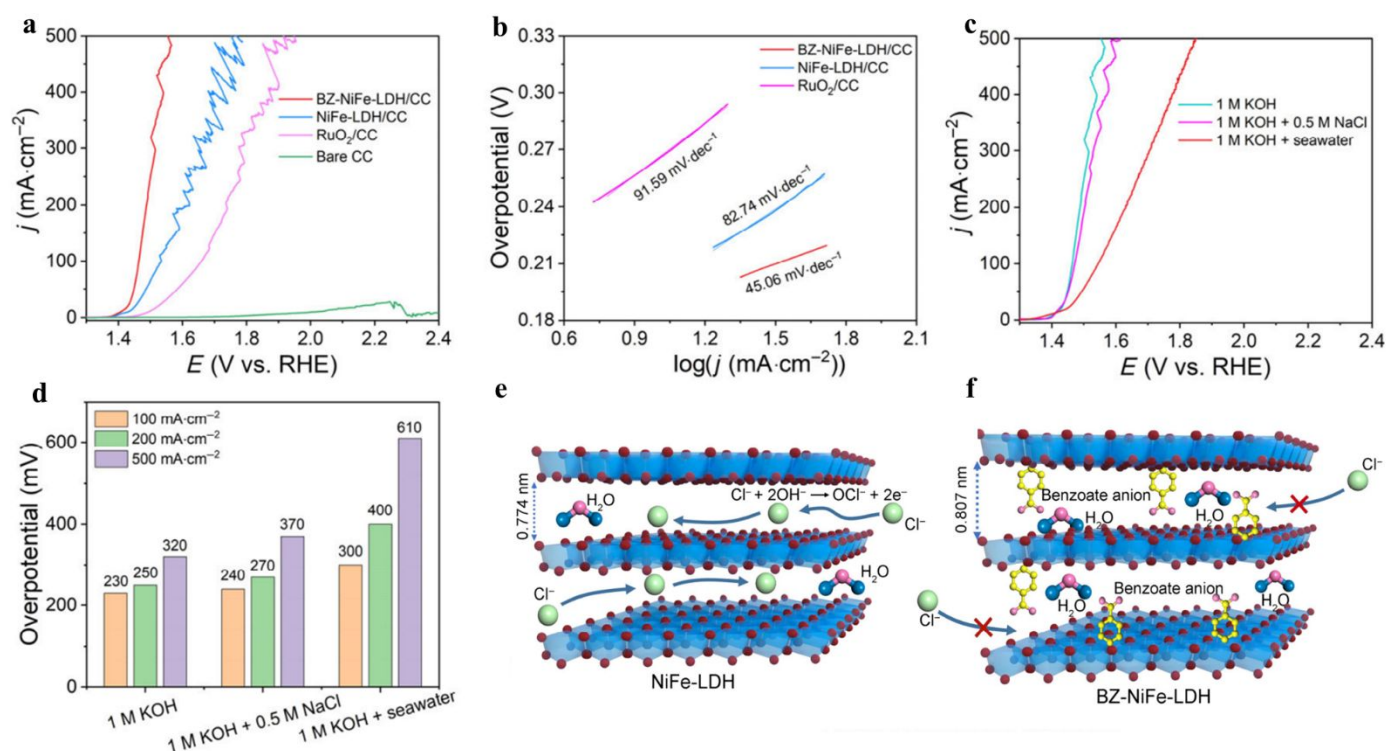


Fig. 12 (a) Polarization curves of different catalysts toward OER in 1 M KOH, and (b) the Tafel plots of different catalysts toward OER. (c) Polarization curves of BZ-NiFe-LDH/CC toward OER in electrolytes of alkaline water, alkaline simulated seawater, and alkaline actual seawater. (d) Comparison of the overpotentials required to achieve the different current densities toward OER for BZ-NiFe-LDH/CC in the electrolytes of alkaline water, alkaline simulated, and alkaline actual seawater. And the schematic pictures of enhanced activity and stability for LDHs in seawater oxidation by the BZ-intercalated strategy: (e) regular NiFe LDH and (f) BZ-intercalated BZ-NiFe-LDH. Adopted with permission from Zhang *et al.*¹⁰⁰ Copyright (2022), SciOpen.

In conclusion, the intercalation of anions enhances the electrocatalytic activity and stability of LDHs in alkaline seawater electrolytes for OER. This improvement can be attributed to the following factors: i) Intercalated anions expand the interlayer space of LDHs, exposing more active sites on the catalyst surface and facilitating the diffusion and penetration of electrolytes. ii) Intercalated anions effectively prevent most chloride ions from occupying the interlayer space, inhibiting unwanted side reactions such as CLER. iii) The presence of intercalated anions influences the metallic active sites within the LDH layers, increasing their electron density and thus enhancing the intrinsic activity of LDHs. iv) Intercalated anions also function as proton acceptors, mitigating the local acidification of the solution to some extent and slowing down the dissolution of LDH electrocatalysts.

4.3. LDH-based electrocatalysts with surface/interface engineering

Various strategies of surficial/interfacial engineering, such as metal loading, morphology modification, and hybridization of LDHs with functional composites, have been employed to address the limitations of bulk LDHs.^{87, 123-129} These strategies aim to enhance the stability and electrocatalytic activity of LDHs in seawater electrocatalysis. The electrocatalytic performance and stability data of LDH-based electrocatalysts prepared using surficial/interfacial engineering for OER, HER, and overall seawater splitting are summarized in **Table 2-4**, respectively.

Table 2. The electrocatalytic activities and stabilities for seawater oxidation over LDH-related electrocatalysts prepared by surficial/interfacial engineering.

Entry	^a OER Electrocatalysts	Electrolytes	η and its corresponding current density	^b Chr Amp	^c Chr Pot	Parameters for service life studies	Refs.
1	B-Co ₂ Fe LDH	Actual seawater + 1 M KOH	245 mV at 10 mA cm ⁻² ; 310 mV at 100 mA cm ⁻²	No	Yes	500 mA cm ⁻² @ 100 h	26
		0.5 M NaCl + 1 M KOH	273 mV at 100 mA cm ⁻²	Yes	No	>97% retention at 20 h	
2	S-NiMoO ₄ @NiFe LDH/NF	Actual seawater + 1 M KOH	315 mV at 100 mA cm ⁻² ; 361 mV at 500 mA cm ⁻²	No	Yes	500 mA cm ⁻² @ 650 h	2
3	NiFe LDH/FeOOH	0.5 M NaCl + 1 M KOH	286.2 mV at 100 mA cm ⁻² ; 239 mV at 10 mA cm ⁻² ;	-	-	-	90
4	Pt-CoFe(II) LDH/NF	Actual seawater + 1 M KOH	302 mV at 100 mA cm ⁻² ; 375 mV at 500 mA cm ⁻²	No	Yes	500 mA cm ⁻² @ 40 h	91
5	S-doped NiFe LDH/CC	0.5 M NaCl + 1 M KOH	296 mV at 100 mA cm ⁻²	No	Yes	100 mA cm ⁻² @ 12 h	85
6	Post-Ni ₂ Fe-LDH/FeNi ₂ S ₄ /NF	Actual seawater + 1 M KOH	271 mV at 100 mA cm ⁻²	No	Yes	50 mA cm ⁻² @ 20 h	73
7	FeOOH-NiCoMo LDH/NF	0.5 M NaCl + 1 M KOH	272 mV at 50 mA cm ⁻²	No	Yes	50 mA cm ⁻² @ 50 h	86
8	NiFe LDH/NiSx/NF	0.5 M NaCl + 1 M KOH	300 mV at 400 mA cm ⁻²	-	-	-	22
		0.5 M NaCl + 1 M KOH	285 mV at 100 mA cm ⁻²	-	-	-	
9	N-CDs/NiFe LDH/NF	1 M NaCl + 1 M KOH	273 mV at 100 mA cm ⁻²	-	-	-	123
		Actual seawater + 1 M KOH	340 mV at 100 mA cm ⁻²	Yes	No	1.98 V@20 h	
10	CeO _{2-x} /CoFe LDH/NF	0.5 M NaCl + 1 M KOH	204 mV at 100 mA cm ⁻²	Yes	No	50 mA cm ⁻² @ 30 h	124
11	Se/NFF/NiFe LDH	1 M NaCl + 1 M KOH	220 mV at 20 mA cm ⁻²	No	Yes	100 mA cm ⁻² @250 h	125
		0.5 M NaCl + 1 M KOH	216 mV at 10 mA cm ⁻² ; 245 mV at 100 mA cm ⁻² ; 293 mV at 1000 mA cm ⁻²	-	-	-	
12	Ag-NiFe LDH/NF	0.5 M NaCl + 1 M KOH	217 mV at 10 mA cm ⁻² ; 246 mV at 100 mA cm ⁻² ; 303 mV at 1000 mA cm ⁻²	-	-	-	72
		Actual seawater + 1 M KOH	266 mV at 500 mA cm ⁻²	No	Yes	1000 mA cm ⁻² @1000 h	
13	NiCo@NiFe/NF	Actual seawater + 1 M KOH	266 mV at 500 mA cm ⁻²	No	Yes	500 mA cm ⁻² @100 h	126
14	BSCF/CeO ₂ /NiFe LDH	0.5 M NaCl + 1 M KOH	297 mV at 100 mA cm ⁻²	No	Yes	100 mA cm ⁻² @100 h	127

^a NF-Ni foam, NFF-NiFe foam, CC-carbon cloth; ^b ChrAmp: Chronoamperometry; ^c ChrPot: Chronopotentiometry.

The addition of metal species can enhance electronic interactions between catalysts and reactants, modulate the 3d orbital energy levels of active metal components, and potentially create oxygen defects, thereby

reducing the surface adsorption energy of intermediates. A notable example is the absorption of platinum ions onto the surface of self-supported CoFe(II) LDH, followed by their reduction to metallic platinum (Pt) through the spontaneous oxidation of Fe²⁺ in CoFe LDH, resulting in the formation of Pt-CoFe LDH electrocatalyst.⁹¹ In this self-assembled Pt-CoFe LDH, the synergistic effect between metallic Pt and CoFe LDH is observed, as the multidimensional CoFe LDH provides a large surface area for Pt anchoring, while the Pd loading enhances the conductivity of CoFe LDH and introduces additional active sites on its surface. Consequently, the obtained Pt-CoFe LDH exhibits remarkable electrocatalytic activity and stability for seawater splitting in real seawater electrolytes, as detailed in **Table 2** (Entry 4), **Table 3** (Entry 3), and **Table 4** (Entry 5). Another study by Liu *et al.* demonstrates the fabrication of an electrocatalyst where Ag nanoparticles are supported on NiFe LDH.⁷² The introduction of Ag significantly enhances the electrocatalytic activity and stability of pristine NiFe LDH, enabling it to achieve a lower overpotential of 303 mV to approach industrial-level current density for seawater oxidation (**Table 2**, Entry 12). The authors attribute the excellent electrocatalytic activity of the Ag-NiFe LDH catalyst in seawater oxidation to the inherent conductivity and active sites of the original NiFe LDH, which are further improved by Ag doping.⁷² Furthermore, DFT calculations presented in this work reveal that the oxidation of Ag stabilizes the reduced lattice oxygen, thereby preventing structural changes in LDH during electrocatalysis and ensuring OER stability.⁷²

Table 3. The electrocatalytic activities and stabilities for HER in the real/simulated seawater electrolytes over LDH-related electrocatalysts prepared by the surficial/interfacial engineering.

Entry	HER Electrocatalysts	Electrolytes	η and its corresponding current density	Chr Amp	Chr Pot	Parameters for service life studies	Refs.
1	S-NiMoO ₄ @NiFe-LDH/NF	0.5 M NaCl + 1 M KOH	170 mV at 100 mA cm ⁻²	Yes	No	slight fluctuation for 20 h	2
		Actual seawater + 1 M KOH	220 mV at 100 mA cm ⁻²	-	-	-	
2	NiFe LDH/FeOOH	0.5 M NaCl + 1 M KOH	181.8 mV at 10 mA cm ⁻²	-	-	-	90
3	Pt-CoFe(II) LDH/NF	Actual seawater + 1 M KOH	21 mV at 10 mA cm ⁻² ; 94 mV at 100 mA cm ⁻² ; 224 mV at 500 mA cm ⁻²	No	Yes	500 mA cm ⁻² @ 40 h	91

The hierarchical structure of a catalyst offers several advantages, including a large surface area for anchoring a greater number of active sites at a multi-dimensional level. Additionally, it significantly enhances mass transfer processes and the penetration of electrolytes. Zhang *et al.* synthesized a hierarchical NiCo@NiFe LDH electrocatalyst with a dendritic core-shell structure, as illustrated in **Fig. 13a-j**.¹²⁶ This catalyst exhibited remarkable performance, requiring overpotentials of only 222 mV and 266 mV to achieve current densities of 100 mA cm⁻² and 500 mA cm⁻², respectively, for seawater oxidation in 1 M KOH electrolytes (**Fig. 13k, l**). Furthermore, the hierarchical NiCo@NiFe LDH demonstrated nearly 100% OER Faradaic efficiency and

maintained long-term stability, as indicated in **Table 2** (Entry 13). The dendritic core-shell structure not only increased the surface area of the catalyst but also improved mass transfer and charge transfer during seawater oxidation. As a result, the NiCo@NiFe LDH with a hierarchical structure exhibited superior stability and electrocatalytic activity compared to regular NiFe LDH electrocatalysts.¹²⁶

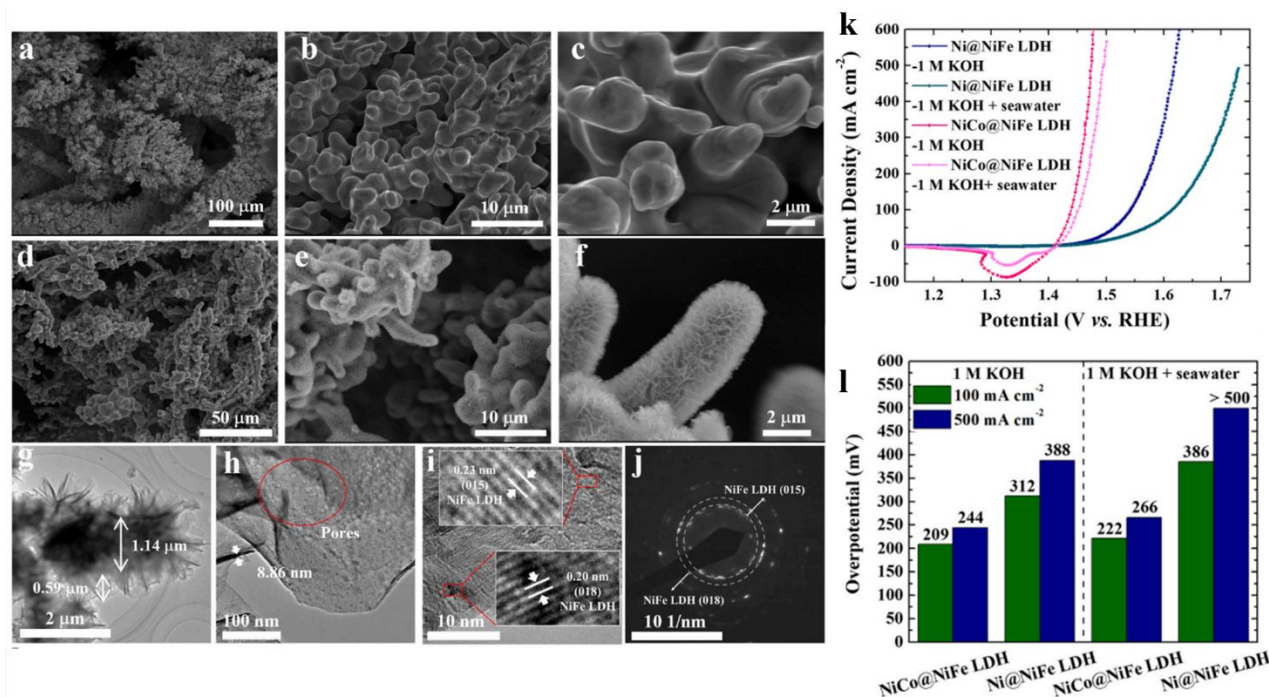


Fig. 13 Scanning electron microscopy images of (a–c) NiCo foam and (d–f) NiCo@NiFe LDH. (g–i) the corresponding Transmission electron microscopy images and (j) the selected area electron diffraction pattern of NiCo@NiFe LDH. (k) OER polarization curves and (l) the overpotentials of as-obtained NiCo@NiFe LDH and Ni@NiFe LDH in different electrolytes. Reprinted with permission.¹²⁶ Copyright (2022), Elsevier Ltd.

The electrocatalytic activity of bulk LDHs is limited by their poor electrical conductivity. While glassy carbon (GC) electrodes can be used to support LDH catalysts and prepare working electrodes, they do not significantly enhance the catalyst's conductivity due to the limited contact area with the LDH film on the surface. Additionally, working electrodes prepared using catalyst ink and GC are not highly stable during seawater electrocatalysis. For instance, NiFe LDH on GC showed high activity but poor stability at pH 9.2 in simulated seawater electrolytes containing borate buffer.²⁷ After just one hour of seawater electrocatalysis at a steady current density of 10 mA cm⁻², the required potential rapidly increased by 0.7 V. To address these challenges, researchers have explored alternative approaches such as directly growing LDH-related electrocatalysts on the surface of materials like metal foam (MF),^{2, 22, 72, 73, 86, 90, 91, 123, 124, 126, 127} carbon cloth (CC),⁸⁵ iron plate (IP),^{93, 94} and more. Experimental results demonstrate that LDHs combined with MF, CC, or IP exhibit superior electrocatalytic performance compared to bulk LDHs, as summarized in **Table 1**.

The construction of multi-layer or heterojunction structures in LDH-related electrocatalysts offers significant improvements in their corrosion resistance for seawater electrocatalysis in both real and simulated seawater electrolytes.¹²⁵ For example, Kuang *et al.* developed a multilayer anode by coating a NiFe-LDH layer on a NiSx layer-modified Ni foam.²² This working electrode demonstrated excellent corrosion resistance and catalytic activity for OER in alkaline seawater splitting, even at industrially necessary current densities (**Table 2**, Entry 8). Jiang *et al.* prepared a NiFe LDH/FeOOH electrocatalyst, which exhibited high electrocatalytic activity and stability for alkaline seawater electrocatalysis, including OER, HER, and full seawater splitting.⁹⁰ Detailed data can be found in **Table 2** (Entry 3), **Table 3** (Entry 2), and **Table 4** (Entry 2). The enhanced activity and corrosion resistance to chloride ions can be attributed to the heterojunction formed between NiFe LDH and FeOOH, which promotes the formation of NiOOH species.⁹⁰

To develop advanced LDH-based electrocatalysts for seawater electrocatalysis, researchers often employ a combination of the aforementioned strategies. For instance, Wang *et al.* synthesized a complex LDH-related composite by using a nickel foam as a support to grow sulfur-modified NiMoO₄ nanorods (S-NiMoO₄), followed by the deposition of a NiFe LDH layer on the surface of S-NiMoO₄.² This composite possesses a hierarchical structure that offers a large surface area for increased active site availability. The incorporation of sulfur doping in the composite enhances its porosity and hydrophilic characteristics. The hybridization of NiFe LDH with NiMoO₄ nanorods leads to incomplete crystallization of LDH, and the presence of partial crystalline structure improves the corrosion resistance of S-NiMoO₄@NiFe-LDH to chloride ions in seawater electrolytes. As a result, this complex LDH-related composite exhibits excellent electrocatalytic activity and superior stability for seawater electrocatalysis, including OER, HER, and overall seawater splitting (refer to **Table 2** (Entry 2), **Table 3** (Entry 1), and **Table 4** (Entry 1) for detailed data, respectively).

In another study, Wu *et al.* prepared a hierarchical nanosheet-nanoflake-structured boron-modified CoFe LDH catalyst with partial crystallinity, which demonstrated outstanding catalytic activity for seawater oxidation (**Table 2**, Entry 1).²⁶ The authors highlighted that the hierarchical structure of the boron-modified CoFe LDH catalyst significantly increases its surface area, providing more accessible active sites compared to the pure nanosheet structure. Additionally, the boron doping reagent used in this work, NaBH₄, with its strong reducing ability, promotes the creation of oxygen defects by capturing O₂ during the synthesis process, resulting in partial crystallinity in the catalyst. This partial crystallinity further enhances electronic kinetics.²⁶ **Table 4.** Cell voltages and their corresponding current densities for full seawater electrocatalysis over LDH-related electrocatalysts prepared by the surficial/interfacial engineering.

Entry	Electrocatalysts	Electrolytes	cell voltage and its corresponding current density	Chr Amp	Chr Pot	Remark after stability test	Refs.
1	S-NiMoO ₄ @NiFe-LDH/NF ^{OER} // S-NiMoO ₄ @NiFe-LDH/NF ^{HER}	0.5 M NaCl + 1 M KOH	1.68 V at 100 mA cm ⁻²	-	-	-	2
		Actual seawater + 1 M KOH	1.73 V at 100 mA cm ⁻²	Yes	No	Reasonable stability at 1.68 V	
2	NiFe LDH/FeOOH ^{OER} // NiFe LDH/FeOOH ^{HER}	0.5 M NaCl + 1 M KOH	1.55 V at 10 mA cm ⁻²	No	Yes	works steadily for 105 h at 100 mA cm ⁻²	90
3	NiFe LDH ^{OER} // NiMoN ^{HER}	Actual seawater + 1 M KOH	1.477 V at 10 mA cm ⁻² ; 1.533 V at 100 mA cm ⁻² ;	No	Yes	good durability over 100 h at 500 mA cm ⁻²	94
			1.665 V at 500 mA cm ⁻²				
4	NiFe LDH/NF ^{OER} // MoNi ₄ /MoO ₂ /NF ^{HER}	Actual seawater + 1 M KOH	1.54 V at 500 mA cm ⁻²	No	Yes	works steadily for 12 h at 100 mA cm ⁻²	75
5	Pt-CoFe(II) LDH/NF ^{OER} // Pt-CoFe(II) LDH/NF ^{HER}	Actual seawater + 1 M KOH	1.518 V at 10 mA cm ⁻² ; 1.651 V at 100 mA cm ⁻² ; 1.858 V at 500 mA cm ⁻²	No	Yes	works steadily for 40 h at 500 mA cm ⁻²	91
6	SSFF@NiFe LDH ^{OER} // SSFF@NiFe LDH ^{HER}	0.5 M NaCl + 1 M KOH	1.76 V at 10 mA cm ⁻² ; 1.90 V at 100 mA cm ⁻²	Yes	No	No decay for 10 h at 1.85 V	128
7	NiCoP/NiCo-LDH ^{OER} // NiCoP/NiCo-LDH ^{HER}	0.5 M NaCl + 1 M KOH	1.66 V at 50 mA cm ⁻²	-	-	-	129
8	NiFe LDH/NiSx/Ni ^{OER} // Ni-NiO-Cr ₂ O ₃ ^{HER}	Actual seawater + 1 M KOH	2.12 V at 400 mA cm ⁻²	No	Yes	works steadily for 1000 h at 400 mA cm ⁻²	22
9	NiFe LDH ^{OER} // Pt nanoparticles ^{HER}	0.5 M NaCl + 0.5 M KOH	1.6 V at 200 mA cm ⁻²	Yes	No	Reasonable stability for 100 h at 1.6V	87
10	Se/NiFe Foam/NiFe LDH ^{OER} // NiMoO ₄ nanowires ^{HER}	1 M NaCl + 1 M KOH	1.6 V at 200 mA cm ⁻²	No	Yes	Negligible decay is obtained for ~45 h operation at 10 mA cm ⁻²	125
11	BSCF@CeO ₂ @NiFe LDH ^{OER} // 20% Pt/C ^{HER}	0.5 M NaCl + 1 M KOH	1.7 V at 100 mA cm ⁻²	No	Yes	slight degradation after a long-term 100 h test at 100 mA cm ⁻²	127
		Actual seawater + 1 M KOH	1.76 V at 100 mA cm ⁻²	-	-	-	

In conclusion, surficial/interfacial engineering strategies, such as metal loading, controlled hierarchical structure preparation, and hybridization of LDHs with functional composites, have been extensively investigated for the design and synthesis of highly efficient and stable LDH-related electrocatalysts for seawater electrocatalysis. Coating LDHs with noble metals has shown significant improvement in the electrocatalytic activities of LDH-related catalysts for OER and HER in both real and simulated seawater electrolytes, as evident from the data in **Tables 2** and **3**. However, the scarcity of noble metals results in increased costs for H₂ production using these electrocatalysts. Comparing the electrocatalytic activities of various synthesized LDH-related catalysts for seawater oxidation in **Table 2**, it appears that CeO_{2-x} could be a promising material for hybridization with LDHs to achieve efficient seawater splitting. Nonetheless, further advancements are required to enhance the stability of LDH-related electrocatalysts in seawater electrocatalysis, particularly at high current densities relevant to industrial-level seawater oxidation (*e.g.*, 1000 mA cm⁻²).

4.4. LDH derivatives using LDHs as precursors

All of the aforementioned studies demonstrate the effectiveness of LDH-related materials as

electrocatalysts for seawater electrocatalysis. However, researchers have recognized the need to go beyond LDH materials alone. In recent years, there has been extensive exploration of LDH derivatives, including metal (oxy)hydroxides^{70, 130} and phosphides,^{131, 132} to inherit the advantages of LDHs and develop new properties. These derivatives can be designed as hybrid active species with hierarchical structures, having the heterogeneous porous interfaces that can accommodate precipitated by-products. Moreover, they offer increased accessible catalytic sites and diffusive channels for efficient gas escape in seawater electrolytes. These LDH derivative-based electrocatalysts exhibit exceptional electrocatalytic activities for OER or HER in seawater electrolytes, as detailed in **Tables 5-7**.

Xiao *et al.* successfully synthesized a polymetallic phosphide material, Fe₂P-NiCoP, using dual precursors: a Fe-based metal-organic framework (MOF) and a NiCo LDH.⁷¹ This Fe₂P-NiCoP material demonstrated excellent bifunctional electrocatalytic performance in seawater electrocatalysis, particularly for overall seawater splitting (**Table 7**, Entry 1). DFT calculations conducted in this study revealed that the reconstructed NiOOH/FeOOH species formed from Fe₂P-NiCoP played a vital role as the active species in seawater electrocatalysis. These active species effectively reduced the adsorption energy of product intermediates, thereby accelerating reaction kinetics and enhancing electrocatalytic efficiency.⁷¹ In a separate study, Huang *et al.* synthesized a hybrid material comprising porous Ni₅P₄ nanosheets and amorphous Ni (oxy)hydroxides (Ni₅P₄@NiOOH/CC).⁶⁹ This hybrid material exhibited superior electrocatalytic performance and durability for HER in actual seawater electrolytes, even without the addition of alkaline additives. Experimental results and theoretical calculations indicated that the synergy between Ni₅P₄ and NiOOH greatly enhanced the electronic interactions between the two catalysts. The decreased bond-breaking energy between phosphorus and adsorbed hydrogen, facilitated by the synergistic effect, resulted in easier water molecule activation and adsorption on the hybrid catalyst. Consequently, the hydrogen adsorption and desorption processes were accelerated, leading to enhanced electrocatalytic activity and stability.⁶⁹ Furthermore, the NiOOH component served as a protective layer, safeguarding the electrode from chloride corrosion.

The 3-dimensional bristlegrass-like Co-doped Ni₂P (Co-Ni₂P) composites were synthesized using NiCo LDH as a precursor, followed by phosphating treatment.¹³³ DFT calculations confirmed that the presence of Co atoms in Co-Ni₂P accelerated water dissociation and facilitated the generation of *H intermediates during seawater electrocatalysis, resulting in improved hydrogen production efficiency.¹³³ Detailed data can be found in **Table 7** (Entry 2). Furthermore, a novel porous feather-like NiCoP holey nanoarray was prepared using NiCo LDH as a precursor.¹³⁴ This NiCoP electrocatalyst demonstrated efficient HER catalytic activity in

actual seawater electrolytes and exhibited long-term durability (**Table 6**, Entry 2). The unique porous 3-dimensional feather-like structure of the NiCoP electrocatalyst provided a larger surface area, enhanced mass transfer, and increased exposure of active sites, thereby contributing to improved HER catalytic performance.¹³⁴

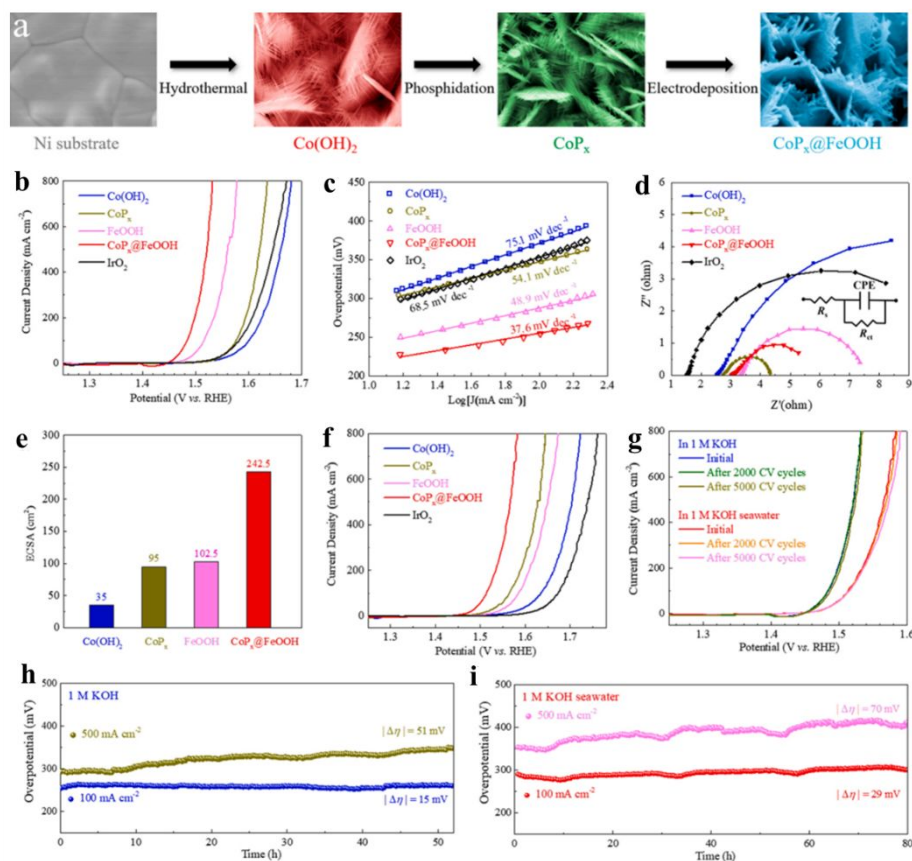


Fig. 14 (a) The synthetic processes of $\text{CoP}_x@FeOOH$. (b) OER polarization curves of various electrocatalysts in alkaline water electrolytes; (c) the corresponding Tafel plots; (d) Nyquist plots; and (e) Electrochemical active surface area (ECSA) values. (f) OER polarization curves of various electrocatalysts in alkaline seawater electrolytes. (g) OER polarization curves of $\text{CoP}_x@FeOOH$ that before and after multiple CV scans in alkaline water/seawater electrolytes. Stability test of $\text{CoP}_x@FeOOH$ electrocatalyst: (h) ChrPot curves in alkaline water electrolytes; (i) ChrPot curves in alkaline seawater electrolytes. Reprinted with permission.¹³¹ Copyright (2021), Elsevier B.V.

Ren's group successfully fabricated a porous sulfur-doped NiFe (oxy)hydroxide (S-NiFeOOH) catalyst with strong hydrophilic characteristics. This catalyst exhibited superior electrocatalytic activity for OER in alkaline seawater electrolytes.¹³⁰ By employing the obtained S-NiFeOOH catalyst as the catalytic anode and nickel foam-supported NiMoN as the cathode in a two-electrode electrolyzer, the entire electrocatalytic system demonstrated effective seawater splitting in actual seawater electrolytes. Detailed activity data can be found

in **Table 7** (Entry 4). The presence of a protective NiFe nitride (NiFeN) on NiMoN nanorods, which could evolve from an amorphous oxide/oxy(hydroxide) layer, helped safeguard the synthesized catalyst against chloride corrosion during seawater oxidation.¹

Additionally, Ren and co-workers illustrated that a bimetallic phosphide electrocatalyst derived from NiFe (oxy)hydroxide exhibited excellent bifunctional electrocatalytic activity for overall seawater splitting in actual seawater electrolytes (**Table 7**, Entry 5).²⁹ Stability tests demonstrated that the electrocatalytic activity of this Ni₂P-Fe₂P electrocatalyst only slightly decreased after approximately 48 h of operation under a current density of 500 mA cm⁻². The same research team synthesized the CoP_x@FeOOH electrocatalyst with a core-shell structure, as depicted in **Fig. 14**.¹³¹ The hierarchical CoP_x@FeOOH electrocatalyst possessed enhanced conductivity, enriched active sites, accelerated bubble-release capability, and optimal absorption energy for OER intermediates. These attributes contributed to its excellent electrocatalytic activity for seawater oxidation. Moreover, when used as an anode catalyst in an electrocatalytic system for overall seawater splitting, the hierarchical CoP_x@FeOOH catalyst exhibited good electrocatalytic activity and stability. The catalytic data for OER and overall seawater splitting can be found in **Table 5** (Entry 1) and **Table 7** (Entry 3), respectively. The superior stability of CoP_x@FeOOH could be attributed to its hierarchical structure and hydrophilic features, which provided sufficient mechanical strength and effective mass transfer during seawater electrocatalysis.¹³¹

In another study by Wan *et al.*, an active OER electrocatalyst, NiFeO_xH_y, was prepared by subjecting pristine NiFe LDH to a 400-cycle voltammetric treatment.⁷⁰ The gradual formation of an amorphous (oxy)hydroxide with Fe during potential cycling significantly enhanced the OER catalytic activity of NiFeO_xH_y compared to NiFe LDH.

Table 5. The electrocatalytic activities and stabilities for the seawater oxidation over the derivatives of LDHs in the real/simulated seawater electrolytes.

Entry	OER Electrocatalysts	Electrolytes	η and its corresponding current density	Chr Amp	Chr Pot	Parameters for service life studies	Refs.
1	CoP _x @FeOOH	Actual seawater + 1 M KOH	235 mV at 10 mA cm ⁻² ; 283 mV at 100 mA cm ⁻² ; 337 mV at 500 mA cm ⁻²	No	Yes	500 mA cm ⁻² @ 80h	131
2	S-NiFeOOH	Actual seawater + 1 M KOH	300 mV at 100 mA cm ⁻² ; 398 mV at 500 mA cm ⁻²	No	Yes	100 mA cm ⁻² @ 100h	130
3	NiFeO _x H _y	0.5 M NaCl + 1 M KOH	280 mV at 100 mA cm ⁻²	No	Yes	500 mA cm ⁻² @ 100h	70
4	B-CoNiOOH/PANI@TiO ₂	0.5 M NaCl + 1 M KOH	398 mV at 100 mA cm ⁻²	Yes	No	1.70V @ 100h	132

Table 6. The electrocatalytic activities and stabilities for HER in the real/simulated seawater electrolytes

over LDH derivatives.

Entry	HER Electrocatalysts	Electrolytes	η and its corresponding current density	Chr Amp	Chr Pot	Parameters for service life studies	Refs.
1	Ni ₅ P ₄ @NiOOH	Actual seawater	144 mV at 10 mA cm ⁻²	No	Yes	100 mA cm ⁻² @ 40 h	69
2	NiCoP	Actual seawater	287 mV at 10 mA cm ⁻²	Yes	No	1.52V@12h	134
3	B-CoNiOOH/PANI@TiO ₂	0.5 M NaCl + 1 M KOH	196 mV at 100 mA cm ⁻²	Yes	No	1.68V@100h	132

Table 7. Electrocatalytic data toward overall seawater splitting over various reported electrocatalysts of LDH derivatives.

Entry	Electrocatalysts	Electrolytes	cell voltage and its corresponding current density	Chr Amp	Chr Pot	Remark after stability test	Refs.
1	Fe ₂ P-NiCoP ^{OER} // Pt/C ^{HER}	Actual seawater + 1 M KOH	1.525 V at 10 mA cm ⁻²	Yes	No	Reasonable stability at 1.49V	71
2	Co-Ni ₂ P ^{OER} // 20% Co-Ni ₂ P ^{HER}	0.5 M NaCl + 1 M KOH	1.71 V at 50 mA cm ⁻²	No	Yes	slight degradation after long-term 22 h test at 100 mA cm ⁻²	133
3	CoP _x @FeOOH ^{OER} // CoP _x ^{HER}	Actual seawater + 1 M KOH	1.71 V at 100 mA cm ⁻² ; 1.87 V at 500 mA cm ⁻²	No	Yes	slight degradation after 100 h test at mA cm ⁻²	131
4	S-NiFeOOH ^{OER} // NiMoN ^{HER}	Actual seawater + 1 M KOH	1.84 V at 500 mA cm ⁻² ; 1.95 V at 1000 mA cm ⁻²	No	Yes	acceptable degradation after 100 h test at 500 mA cm ⁻²	130
5	Ni ₂ P-Fe ₂ P/NF ^{OER} // Ni ₂ P-Fe ₂ P/NF ^{HER}	Actual seawater + 1 M KOH	1.81 V at 100 mA cm ⁻² ; 2.00 V at 500 mA cm ⁻²	No	Yes	slight degradation after 48 h test at 500 mA cm ⁻²	29
6	NiFeO _x H _y ^{OER} // Pt/C ^{HER}	0.5 M NaCl + 1 M KOH	2.2 V at ~250 mA cm ⁻²	No	Yes	slight degradation after 100 h test at 500 mA cm ⁻²	70
7	B-CoNiOOH/PANI@TiO ₂ ^{OER} // B-CoNiOOH/PANI@TiO ₂ ^{HER}	0.5 M NaCl + 1 M KOH	1.87 V at 100 mA cm ⁻²	Yes	No	reasonable degradation after 72 h test at 2.08V	132

To facilitate a more intuitive comparison of the electrocatalytic activity of different LDH-related electrocatalysts for OER, HER, and overall seawater splitting, selected data from **Table 1-7** were used to create a histogram and scatterplot, as depicted in **Fig. 15**. **Fig. 15a, b** illustrate the overpotentials required to achieve a current density of 100 mA cm⁻² for OER over various LDH-related electrocatalysts in alkaline actual seawater and simulated water, respectively. The Ag-NiFe LDH/NF⁷² and LDH/NFF¹¹⁶ exhibit lower overpotentials for seawater oxidation in both alkaline actual seawater and simulated seawater, suggesting that noble metal doping and integration of catalysts with hierarchical conductive substrates are effective strategies to enhance the OER catalytic activity of LDH-related catalysts. While numerous LDH-related catalysts have been developed for seawater oxidation, there have been fewer studies focusing on LDH-related catalysts for HER. As demonstrated in **Fig. 15c**, the Pt-CoFe(II)LDH/NF⁷² displays the best HER activity compared to S-NiMoO₄@NiFe-LDH/NF² and B-CoNiOOH/PANI@TiO₂¹³². This indicates that noble metal doping can significantly improve the HER performance of LDH-related catalysts in seawater electrocatalysis. **Fig. 15d**

presents the cell voltages required for alkaline seawater splitting to achieve a current density of 100 mA cm^{-2} using various two-electrode systems based on LDH-related electrocatalysts. It can be observed that the NiFe LDH OER // NiMoN HER⁹⁴ configuration is one of the most efficient two-electrode electrolyzers compared to other LDH-related electrocatalyst-based electrolyzers.

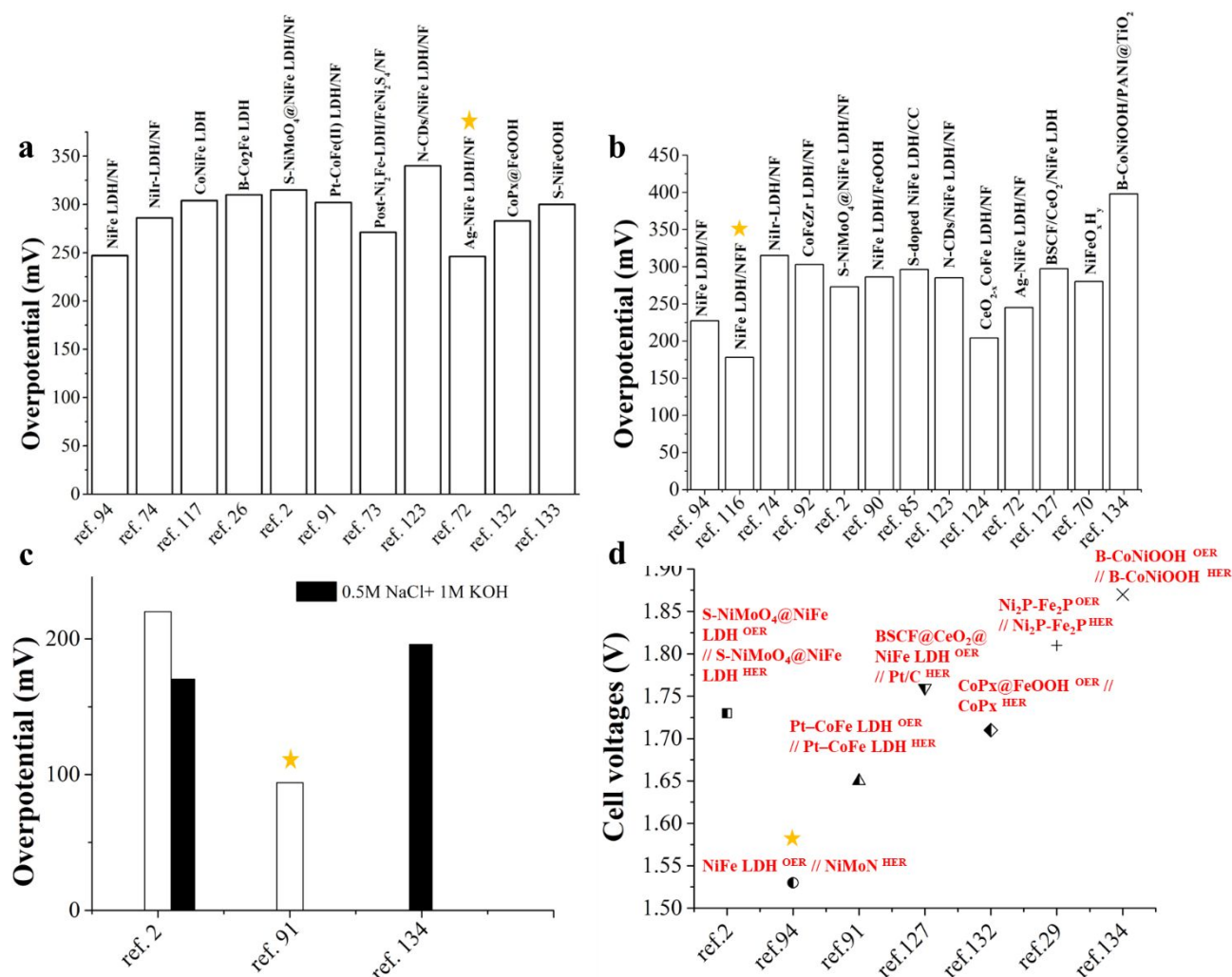


Fig. 15 (a) Overpotential of various LDH-related electrocatalysts at 100 mA cm^{-2} for OER in actual seawater + 1M KOH. (b) Overpotential of various LDH-related electrocatalysts at 100 mA cm^{-2} for OER in 0.5M NaCl + 1M KOH. (c) Overpotential of various LDH-related electrocatalysts at 100 mA cm^{-2} for HER. The white bar indicates that the electrolyte used in the reaction is actual seawater + 1M KOH, while the black bar indicates the electrolyte is 0.5M NaCl + 1M KOH. (d) The cell voltages needed in alkaline seawater splitting to deliver the current density of 100 mA cm^{-2} for various LDH-related electrocatalysts.

While there have been some promising advancements, there is still ample opportunity for the design and synthesis of LDH derivatives in the realm of seawater electrocatalysis. To explore further possibilities in this field, it is necessary to develop a wider range of LDH derivatives, including mixed metal oxides, bimetal

nitrides, bimetal sulfides, and bimetal selenides. These derivatives should be specifically aimed at enhancing the catalytic activity of HER and OER, while simultaneously exhibiting robust resistance to chlorine corrosion in seawater electrolytes.

5. Summary and Outlook

Seawater resources are abundant on Earth, providing nearly limitless potential for direct seawater electrocatalysis and the generation of green hydrogen energy. The technology to produce hydrogen and oxygen directly from seawater holds great promise and is considered environmentally friendly. Particularly in arid regions, the combination of this technology with fuel cells can produce fresh water, which holds significant implications for drought relief. However, the sluggish kinetics of OER and HER, as well as issues like chlorine oxidation and chlorine corrosion during seawater electrocatalysis, pose significant challenges to the widespread adoption of this technology. Researchers have been diligently working to address these issues by designing and fabricating advanced electrocatalysts that exhibit long-term stability and resistance to chloride corrosion in seawater splitting. LDH-based catalysts have garnered considerable attention in recent years due to their low cost and unique properties. In this review, we present the synthesis methods and characterization techniques for LDH electrocatalysts, followed by an overview of the latest progress in the application of LDH-based electrocatalysts for seawater electrocatalysis. We summarize five strategies for enhancing the OER/HER/overall seawater splitting activity of LDH materials: 1) Utilizing electrolyte additives to enhance the electrocatalytic activity and anti-corrosion ability of LDH-based catalysts; 2) Tuning the metal cations in the brucite-like layer of LDHs, including the choice of metal type and the ratio of metal cations. It has been observed that Ni-based LDHs exhibit higher OER activity thus far; 3) Intercalating new anions to increase the interlayer spacing, improving seawater mass transfer and repelling chloride ions during seawater electrocatalysis; 4) Employing surface/interface engineering methods such as cation doping, morphology modification, and hybridization of LDHs with conductive composites to effectively enhance conductivity, surface area, and electronic structure, as well as facilitate electrolyte penetration and mass transfer processes of LDH-based catalysts, leading to improved OER/HER activity; 5) Exploring LDH derivatives such as metal (oxy)hydroxides and phosphides that not only inherit the unique properties of LDHs but also offer additional advantages. For instance, the presence of phosphorus in LDH derivatives enhances the processes of hydrogen adsorption and desorption compared to pristine LDHs, resulting in improved HER activity.

Direct seawater electrocatalysis is an emerging technology that is still in its infancy. Consequently, there remain critical challenges in the design and synthesis of LDH-related electrocatalysts for efficient seawater splitting that must be addressed in the future. The challenges and potential solutions are outlined below:

1. The first challenge is to fabricate advanced LDH-related catalysts with enhanced HER/OER activity in seawater electrolytes. Higher activity is crucial not only for H₂ production but also for suppressing undesired side reactions that can generate toxic compounds and corrode the electrode. Despite some promising results in previous research, there is ample opportunity for designing advanced LDH-related electrocatalysts. For instance, the incorporation of machine learning and high-entropy approaches into LDH derivative synthesis, along with the utilization of artificial intelligence to reduce time and cost, is expected to enable the synthesis of novel composite-type LDH derivatives for seawater splitting in the future.

2. Inherent stability constraints exist for LDH-related electrocatalysts, necessitating further studies to enhance their corrosion resistance. Possible strategies include integrating LDHs with anti-chlorine layers, tuning the electronic structures and interactions between catalyst components to improve corrosion resistance, and introducing external ions to modify the chemical environment in the interlayer and reduce Cl⁻ accessibility to the catalytic sites.

3. Although some progress has been made in the development of LDH-related electrocatalysts for seawater electrocatalysis, there is still a lack of understanding regarding their mechanism in natural seawater. To gain in-depth insights into the seawater electrocatalysis mechanism over LDH-related electrocatalysts, a combination of DFT calculation and *in situ* characterization techniques can be employed to investigate structural changes and the adsorption-desorption behavior of OER/HER/CLER intermediates during seawater splitting.

4. Identifying and integrating the OER- and HER-active centers of LDH-related electrocatalysts, as well as designing LDH derivatives with multiple active components for bifunctional seawater electrocatalysis, is crucial for future advancements in LDH-related electrocatalysts. To address this, it is important to rationally design a hierarchical structure for LDH-related electrocatalysts that can effectively hold OER/HER active centers together, ensure good ion transportation between the two centers, and prevent mutual inactivation.

5. Considering the environmental and economic costs of practical applications, a rational cascade of renewable power sources (*e.g.*, solar energy, wind energy) with seawater electrolyzers is highly

desired. It is strongly recommended to cascade LDH-related electrocatalysts with photoelectric devices.

In summary, the current research on LDH-related electrocatalysts for direct seawater electrocatalysis is still limited. Further investigation is required to develop LDH-related electrocatalysts that exhibit high selectivity towards OER and possess long-term stability at high current densities during seawater splitting. Additionally, urgent attention is needed to understand the reaction mechanisms of LDH-related catalysts for OER and HER in real seawater electrolytes. With careful catalyst/device design and a deeper understanding of the mechanisms involved, LDH-related catalysts hold the potential for excellent performance in green hydrogen production, thereby optimizing the global energy landscape.

Acknowledgments

This work was financially supported by the National Natural Science Foundation of China (51909066) and the JST-ERATO Yamauchi Materials Space-Tectonics Project (Grant Number: JPMJER2003).

Author Contributions

All authors have reviewed and edited the manuscript, and agreed the submission of the paper.

References

1. L. Yu, Q. Zhu, S. Song, B. McElhenny, D. Wang, C. Wu, Z. Qin, J. Bao, Y. Yu, S. Chen, Z. Ren, *Nat. Commun.* 2019, **10**, 5106.
2. H. Wang, L. Chen, L. Tan, X. Liu, Y. Wen, W. Hou, T. Zhan, *J. Colloid Interface Sci.* 2022, **613**, 349.
3. G. Cipriani, V.D. Dio, F. Genduso, D.L. Cascia, R. Liga, R. Miceli, G.R. Galluzzo, *Int. J. Hydrogen Energy.* 2014, **39**, 8482.
4. C. Philibert, Producing industrial hydrogen from renewable energy, <https://www.iea.org/commentaries/producing-industrial-hydrogen-from-renewable-energy>, accessed: April, 2017.
5. F. Birol, The future of hydrogen: seizing today's opportunities, <https://www.iea.org/events/the-future-of-hydrogen-seizing-todays-opportunities>, accessed: June, 2019.
6. M.A. Khan, T. Al-Attas, S. Roy, M.M. Rahman, N. Ghaffour, V. Thangadurai, S. Larter, J. Hu, P.M. Ajayan, M.G. Kibria, *Energ. Environ. Sci.* 2021, **14**, 4831.
7. H. Idriss, *Energy Technol.* 2021, **9**, 2000843.
8. X. Zou, Y. Zhang, *Chem. Soc. Rev.* 2015, **44**, 5148.
9. J.A. Turner, *Science.* 2004, **305**, 972.
10. R. Daiyan, I. MacGill, R. Amal, *ACS Energy Lett.* 2020, **5**, 3843.
11. E. Papadis, G. Tsatsaronis, *Energy*, 2020, **205**, 118025.
12. S. van Renssen, *Nat. Clim. Change.* 2020, **10**, 799.
13. J. Cai, J. Ding, D. Wei, X. Xie, B. Li, S. Lu, J. Zhang, Y. Liu, Q. Cai, S. Zang, *Adv. Energy Mater.* 2021, **11**, 2100141.
14. H. Zhou, F. Yu, Q. Zhu, J. Sun, F. Qin, L. Yu, J. Bao, Y. Yu, S. Chen, Z. Ren, *Energ. Environ. Sci.* 2018, **11**, 2858.
15. L. Hui, Y. Xue, B. Huang, H. Yu, C. Zhang, D. Zhang, D. Jia, Y. Zhao, Y. Li, H. Liu, Y. Li, *Nat. Commun.* 2018, **9**, 5309.
16. L. Yu, H. Zhou, J. Sun, F. Qin, F. Yu, J. Bao, Y. Yu, S. Chen, Z. Ren, *Energ. Environ. Sci.* 2017, **10**, 1820.
17. C. Ros, S. Murcia-López, X. Garcia, M. Rosado, J. Arbiol, J. Llorca, J.R. Morante, *ChemSusChem.* 2021, **14**, 2872.

18. W. Tong, M. Forster, F. Dionigi, S. Dresp, R. Sadeghi Erami, P. Strasser, A.J. Cowan, P. Farràs, *Nat. Energy*. 2020, **5**, 367.
19. X. Niu, Q. Tang, B. He, P. Yang, *Electrochim Acta*. 2016, **208**, 180.
20. R. d'Amore-Domenech, Ó. Santiago, T.J. Leo, *Renew. Sust. Energ. Rev.* 2020, **133**, 110166.
21. W. Zheng, L.Y.S. Lee, K.-Y. Wong, *Nanoscale*. 2021, **13**, 15177.
22. Y. Kuang, M.J. Kenney, Y. Meng, W.-H. Hung, Y. Liu, J.E. Huang, R. Prasanna, P. Li, Y. Li, L. Wang, M.-C. Lin, M.D. McGehee, X. Sun, H. Dai, *Proc. Natl. Acad. Sci.* 2019, **116**, 6624.
23. T. Hisatomi, K. Domen, *Nat. Catal.* 2019, **2**, 387.
24. S. Dresp, F. Dionigi, M. Klingenhof, T. Merzdorf, H. Schmies, J. Drnec, A. Poulain, P. Strasser, *ACS Catal.* 2021, **11**, 6800.
25. S. Dresp, F. Dionigi, M. Klingenhof, P. Strasser, *ACS Energy Lett.* 2019, **4**, 933.
26. L. Wu, L. Yu, Q. Zhu, B. McElhenny, F. Zhang, C. Wu, X. Xing, J. Bao, S. Chen, Z. Ren, *Nano Energy*. 2021, **83**, 105838.
27. F. Dionigi, T. Reier, Z. Pawolek, M. Gliech, P. Strasser, *ChemSusChem*. 2016, **9**, 962.
28. X. Yu, Z.-Y. Yu, X.-L. Zhang, Y.-R. Zheng, Y. Duan, Q. Gao, R. Wu, B. Sun, M.-R. Gao, G. Wang, S.-H. Yu, *J. Am. Chem. Soc.* 2019, **141**, 7537.
29. L. Wu, L. Yu, F. Zhang, B. McElhenny, D. Luo, A. Karim, S. Chen, Z. Ren, *Adv. Funct. Mater.* 2021, **31**, 2006484.
30. M. Maril, J.-L. Delplancke, N. Cisternas, P. Tobosque, Y. Maril, C. Carrasco, *Int. J. Hydrogen Energy*. 2022, **47**, 3532.
31. T. Li, H.N. Miras, Y.-F. Song, *Catalysts*. 2017, **7**, 260.
32. M. Al Jaber, M. Mallet, H.C. Greenwell, M. Abdelmoula, C. Ruby, *Appl. Clay Sci.* 2019, **182**, 105281.
33. S.F. Almojil, M.A. Othman, *Sci. Rep.* 2019, **9**, 15511.
34. E.M. Seftel, R.G. Ciocarlan, B. Michielsen, V. Meynen, S. Mullens, P. Cool, *Appl. Clay. Sci.* 2018, **165**, 234.
35. C.V. Luengo, M.A. Volpe, M.J. Avena, *J. Environ. Chem. Eng.* 2017, **5**, 4656.
36. K. Kaneda, T. Mizugaki, *Green Chem.* 2019, **21**, 1361.
37. Y. Wang, D. Yan, S. El Hankari, Y. Zou, S. Wang, *Adv. Sci.* 2018, **5**, 1800064.
38. Q. Chen, Y. Yu, J. Li, H. Nan, S. Luo, C. Jia, P. Deng, S. Zhong, X. Tian, *ChemElectroChem*. 2022, **9**, 202101387.

39. S. Miyata, T. Hirose, *Clay. Clay Miner.* 1978, **26**, 441.
40. Z. Matusinovic, C.A. Wilkie, *J. Mater. Chem.* 2012, **22**, 18701.
41. J. Li, B. Li, J. Wang, L. He, Y. Zhao, *Acta. Chim. Sinica. Acta.* 2021, **79**, 238.
42. Y. Hou, M.R. Lohe, J. Zhang, S. Liu, X. Zhuang, X. Feng, *Energ. Environ. Sci.* 2016, **9**, 478.
43. P. Li, X. Duan, Y. Kuang, Y. Li, G. Zhang, W. Liu, X. Sun, *Adv. Energy Mater.* 2018, **8**, 1703341.
44. R. Li, Y. Wang, W. Li, S. Zhou, P. Tian, H. Gao, X. Liu, J. Zang, *Chem. Commun.* 2019, **55**, 13370.
45. J. Bao, Z. Wang, J. Xie, L. Xu, F. Lei, M. Guan, Y. Zhao, Y. Huang, H. Li, *Chem. Commun.* 2019, **55**, 3521.
46. H. Sun, W. Zhang, J.-G. Li, Z. Li, X. Ao, K.-H. Xue, K.K. Ostrikov, J. Tang, C. Wang, *Appl. Catal. B.* 2021, **284**, 119740.
47. A.-L. Wang, H. Xu, G.-R. Li, *ACS Energy Lett.* 2016, **1**, 445.
48. K. Fan, H. Chen, Y. Ji, H. Huang, P.M. Claesson, Q. Daniel, B. Philippe, H. Rensmo, F. Li, Y. Luo, L. Sun, *Nat. Commun.* 2016, **7**, 11981.
49. Q. Xie, Z. Cai, P. Li, D. Zhou, Y. Bi, X. Xiong, E. Hu, Y. Li, Y. Kuang, X. Sun, *Nano Res.* 2018, **11**, 4524.
50. F. Dionigi, J. Zhu, Z. Zeng, T. Merzdorf, H. Sarodnik, M. Gliech, L. Pan, W.-X. Li, J. Greeley, P. Strasser, *Angew. Chem. Int. Ed. Engl.* 2021, **60**, 14446.
51. F. Dionigi, Z. Zeng, I. Sinev, T. Merzdorf, S. Deshpande, M.B. Lopez, S. Kunze, I. Zegkinoglou, H. Sarodnik, D. Fan, A. Bergmann, J. Drnec, J.F.d. Araujo, M. Gliech, D. Teschner, J. Zhu, W.-X. Li, J. Greeley, B.R. Cuenya, P. Strasser, *Nat. Commun.* 2020, **11**, 2522.
52. L. Yu, H. Zhou, J. Sun, F. Qin, D. Luo, L. Xie, F. Yu, J. Bao, Y. Li, Y. Yu, S. Chen, Z. Ren, *Nano Energy.* 2017, **41**, 327.
53. X. Lu, C. Zhao, *Nat. Commun.* 2015, **6**, 6616.
54. X. Zou, A. Goswami, T. Asefa, *J. Am. Chem. Soc.* 2013, **135**, 17242.
55. P. Li, M. Wang, X. Duan, L. Zheng, X. Cheng, Y. Zhang, Y. Kuang, Y. Li, Q. Ma, Z. Feng, W. Liu, X. Sun, *Nat. Commun.* 2019, **10**, 1711.
56. H. Zhang, X. Li, A. Hähnel, V. Naumann, C. Lin, S. Azimi, S.L. Schweizer, A.W. Maijenburg, R.B. Wehrspohn, *Adv. Funct. Mater.* 2018, **28**, 1706847.
57. H. Yang, Z. Chen, P. Guo, B. Fei, R. Wu, *Appl. Catal. B.* 2020, **261**, 118240.
58. D. Wang, Q. Li, C. Han, Q. Lu, Z. Xing, X. Yang, *Nat. Commun.* 2019, **10**, 3899.

59. M. Gong, Y. Li, H. Wang, Y. Liang, J.Z. Wu, J. Zhou, J. Wang, T. Regier, F. Wei, H. Dai, *J. Am. Chem. Soc.* 2013, **135**, 8452.
60. Y. Lee, J. Suntivich, K.J. May, E.E. Perry, Y. Shao-Horn, *J. Phys. Chem. Lett.* 2012, **3**, 399.
61. T. Audichon, T.W. Napporn, C. Canaff, C. Morais, C. Comminges, K.B. Kokoh, *J. Phys. Chem. C.* 2016, **120**, 2562.
62. P.A. DeSario, C.N. Chervin, E.S. Nelson, M.B. Sassin, D.R. Rolison, *ACS Appl. Mater. Interfaces.* 2017, **9**, 2387.
63. H. Xu, H. Shang, C. Wang, Y. Du, *Adv. Funct. Mater.* 2020, **30**, 2000793.
64. L. Lv, Z. Yang, K. Chen, C. Wang, Y. Xiong, *Adv. Energy Mater.* 2019, **9**, 1803358.
65. S. Anantharaj, V. Aravindan, *Adv. Energy Mater.* 2020, **10**, 1902666.
66. X. Zou, J. Su, R. Silva, A. Goswami, B.R. Sathe, T. Asefa, *Chem. Commun.* 2013, **49**, 7522.
67. J. Wang, H.-x. Zhong, Y.-l. Qin, X.-b. Zhang, *Angew. Chem. Int. Ed. Engl.* 2013, **52**, 5248.
68. G. Liu, Y. Xu, T. Yang, L. Jiang, *Nano Mater. Sci.* 2020, **5**, 101-116.
69. Y. Huang, L. Hu, R. Liu, Y. Hu, T. Xiong, W. Qiu, M.S. Balogun, A. Pan, Y. Tong, *Appl. Catal. B.* 2019, **251**, 181.
70. S. Wan, X. Wang, G. Zhang, Y. Wang, J. Chen, Q. Li, Y. Zhang, L. Chen, X. Wang, G. Meng, K. Jiang, *ACS Sust. Chem. Eng.* 2022, **10**, 11232.
71. M. Xiao, C. Zhang, P. Wang, W. Zeng, J. Zhu, Y. Li, W. Peng, Q. Liu, H. Xu, Y. Zhao, H. Li, L. Chen, J. Yu, S. Mu, *Mater. Today Phys.* 2022, **24**, 100684.
72. S. Liu, S. Ren, R.T. Gao, X. Liu, L. Wang, *Nano Energy.* 2022, **98**, 107212.
73. L. Tan, J. Yu, C. Wang, H. Wang, X. Liu, H. Gao, L. Xin, D. Liu, W. Hou, T. Zhan, *Adv. Funct. Mater.* 2022, **32**, 2200951.
74. H. You, D. Wu, D. Si, M. Cao, F. Sun, H. Zhang, H. Wang, T.-F. Liu, R. Cao, *J. Am. Chem. Soc.* 2022, **144**, 9254.
75. Q. Tu, W. Liu, M. Jiang, W. Wang, Q. Kang, P. Wang, W. Zhou, F. Zhou, *ACS Appl. Energy Mater.* 2021, **4**, 4630.
76. F. Cheng, X. Feng, X. Chen, W. Lin, J. Rong, W. Yang, *Electrochim. Acta.* 2017, **251**, 336.
77. J.W. Boclair, P.S. Braterman, *Chem. Mater.* 1999, **11**, 298.
78. J.W. Boclair, P.S. Braterman, J. Jiang, S. Lou, F. Yarberry, *Chem. Mater.* 1999, **11**, 303.
79. S. Nishimura, A. Takagaki, K. Ebitani, *Green Chem.* 2013, **15**, 2026.

80. G. Dong, F. Xie, F. Kou, T. Chen, F. Wang, Y. Zhou, K. Wu, S. Du, M. Fang, J.C. Ho, *Mater. Today Energy*. 2021, **22**, 100883.
81. W.H. Shaw, J.J. Bordeaux, *J. Am. Chem. Soc.* 1955, **77**, 4729.
82. J.-M. Oh, S.-H. Hwang, J.-H. Choy, *Solid State Ionics*. 2002, **151**, 285.
83. Z. Lu, W. Xu, W. Zhu, Q. Yang, X. Lei, J. Liu, Y. Li, X. Sun, X. Duan, *Chem. Commun.* 2014, **50**, 6479.
84. J. Luo, J.-H. Im, M.T. Mayer, M. Schreier, M.K. Nazeeruddin, N.-G. Park, S.D. Tilley, H.J. Fan, M. Grätzel, *Science*. 2014, **345**, 1593.
85. S.Y. Jung, S. Kang, K.M. Kim, S. Mhin, J.C. Kim, S.J. Kim, E. Enkhtuvshin, S. Choi, H. Han, *Appl. Surf. Sci.* 2021, **568**, 150965.
86. H. Luo, J. Liang, J. Zhou, Z. Yin, Z. Zhang, X. Liu, *New J. Chem.* 2022, **46**, 7999.
87. S. Dresch, F. Dionigi, S. Loos, J. F. d. Araujo, C. Spöri, M. Gliech, H. Dau, P. Strasser, *Adv. Energy Mater.* 2018, **8**, 1800338.
88. Z. Li, M. Shao, H. An, Z. Wang, S. Xu, M. Wei, D.G. Evans, X. Duan, *Chem. Sci.* 2015, **6**, 6624.
89. Z. Yin, R. He, Y. Zhang, L. Feng, X. Wu, T. Wågberg, G. Hu, *J. Energy. Chem.* 2022, **69**, 585.
90. K. Jiang, W. Liu, W. Lai, M. Wang, Q. Li, Z. Wang, J. Yuan, Y. Deng, J. Bao, H. Ji, *Inorg. Chem.* 2021, **60**, 17371.
91. J. Wu, Z. Nie, R. Xie, X. Hu, Y. Yu, N. Yang, *J. Power Sources*. 2022, **532**, 231353.
92. W. Liu, K. Jiang, Y. Hu, Q. Li, Y. Deng, J. Bao, Y. Lei, *J. Colloid Interface Sci.* 2021, **604**, 767.
93. Y. Liu, X. Liang, L. Gu, Y. Zhang, G.-D. Li, X. Zou, J.-S. Chen, *Nat. Commun.* 2018, **9**, 2609.
94. M. Ning, L. Wu, F. Zhang, D. Wang, S. Song, T. Tong, J. Bao, S. Chen, L. Yu, Z. Ren, *Mater. Today Phys.* 2021, **19**, 100419.
95. J.D. Blakemore, H.B. Gray, J.R. Winkler, A.M. Müller, *ACS Catal.* 2013, **3**, 2497.
96. B.M. Hunter, J.D. Blakemore, M. Deimund, H.B. Gray, J.R. Winkler, A.M. Müller, *J. Am. Chem. Soc.* 2014, **136**, 13118.
97. P.J. Sideris, F. Blanc, Z. Gan, C.P. Grey, *Chem. Mater.* 2012, **24**, 2449.
98. P.J. Sideris, U.G. Nielsen, Z. Gan, C.P. Grey, *Science*. 2008, **321**, 113.
99. L. Zhao, Z. Qi, F. Blanc, G. Yu, M. Wang, N. Xue, X. Ke, X. Guo, W. Ding, C.P. Grey, L. Peng, *Adv. Funct. Mater.* 2014, **24**, 1696.

100. L. Zhang, J. Liang, L. Yue, K. Dong, J. Li, D. Zhao, Z. Li, S. Sun, Y. Luo, Q. Liu, G. Cui, A.A. Alshehri, X. Guo, X. Sun, *Nano Res. Energy*. 2022, **1**.
101. Q. Li, F. Huang, S. Li, H. Zhang, X.-Y. Yu, *Small*. 2022, **18**, 2104323.
102. N. Garcia-Araez, V. Climent, J. Feliu, *J. Phys. Chem. C*. 2009, **113**, 9290.
103. S. Hou, L. Xu, X. Ding, R.M. Kluge, T.K. Sarpey, R.W. Haid, B. Garlyyev, S. Mukherjee, J. Warnan, M. Koch, S. Zhang, W. Li, A.S. Bandarenka, R.A. Fischer, *Angew. Chem. Int. Ed. Engl.* 2022, **61**, e202201610.
104. D. Scieszka, J. Yun, A.S. Bandarenka, *ACS Appl. Mater. Interfaces*. 2017, **9**, 20213.
105. D. Scieszka, C. Sohr, P. Scheibenbogen, P. Marzak, J. Yun, Y. Liang, J. Fichtner, A.S. Bandarenka, *ACS Appl. Mater. Interfaces*. 2018, **10**, 21688.
106. T.C. Nagaiah, A. Tiwari, M. Kumar, D. Scieszka, A.S. Bandarenka, *ACS Appl. Energy Mater.* 2020, **3**, 9151.
107. T. Ma, W. Xu, B. Li, X. Chen, J. Zhao, S. Wan, K. Jiang, S. Zhang, Z. Wang, Z. Tian, Z. Lu, L. Chen, *Angew. Chem. Int. Ed. Engl.* 2021, **60**, 22740.
108. M. Yu, J. Li, F. Liu, J. Liu, W. Xu, H. Hu, X. Chen, W. Wang, F. Cheng, *J. Energy Chem.* 2022, **72**, 361.
109. J. Zaffran, M.B. Stevens, C.D.M. Trang, M. Nagli, M. Shehadeh, S.W. Boettcher, M. Caspary Toroker, *Chem. Mater.* 2017, **29**, 4761.
110. Z. Wang, W. Liu, Y. Hu, L. Xu, M. Guan, J. Qiu, Y. Huang, J. Bao, H. Li, *Inorg. Chem. Front.* 2019, **6**, 1890.
111. S. Khatun, P. Roy, *Chem. Commun.* 2022, **58**, 1104.
112. C.-C. Hu, Y.-R. Wu, *Mater. Chem. Phys.* 2003, **82**, 588.
113. E. Potvin, L. Brossard, *Mater. Chem. Phys.* 1992, **31**, 311.
114. R.N. Singh, J.P. Pandey, K.L. Anitha, *Int. J. Hydrogen Energy*. 1993, **18**, 467.
115. S. Dresp, T. Ngo Thanh, M. Klingenhof, S. Brückner, P. Hauke, P. Strasser, *Energ. Environ. Sci.* 2020, **13**, 1725.
116. S. Duan, Z. Liu, H. Zhuo, T. Wang, J. Liu, L. Wang, J. Liang, J. Han, Y. Huang, Q. Li, *Nanoscale*. 2020, **12**, 21743.
117. Y.S. Park, J.-Y. Jeong, M.J. Jang, C.-Y. Kwon, G.H. Kim, J. Jeong, J.-h. Lee, J. Lee, S.M. Choi, *J. Energy Chem.* 2022, **75**, 127.

118. D. Zhou, Z. Cai, Y. Bi, W. Tian, M. Luo, Q. Zhang, Q. Zhang, Q. Xie, J. Wang, Y. Li, Y. Kuang, X. Duan, M. Bajdich, S. Siahrostami, X. Sun, *Nano Res.* 2018, **11**, 1358.
119. X. Ge, C.D. Gu, X.L. Wang, J.P. Tu, *J. Mater. Chem. A.* 2014, **2**, 17066.
120. J.A. Carrasco, R. Sanchis-Gual, A.S.-D. Silva, G. Abellán, E. Coronado, *Chem. Mater.* 2019, **31**, 6798.
121. Y. Dong, S. Komarneni, F. Zhang, N. Wang, M. Terrones, W. Hu, W. Huang, *Appl. Catal. B.* 2020, **263**, 118343.
122. B.M. Hunter, W. Hieringer, J.R. Winkler, H.B. Gray, A.M. Müller, *Energ. Environ. Sci.* 2016, **9**, 1734.
123. P. Ding, H. Song, J. Chang, S. Lu, *Nano Res.* 2022, **15**, 7063.
124. Y. Hu, W. Liu, K. Jiang, L. Xu, M. Guan, J. Bao, H. Ji, H. Li, *Inorg. Chem. Front.* 2020, **7**, 4461.
125. W.H. Hung, B.Y. Xue, T.M. Lin, S.Y. Lu, I.Y. Tsao, *Mater. Today Energy.* 2021, **19**, 100575.
126. F. Zhang, Y. Liu, L. Wu, M. Ning, S. Song, X. Xiao, V.G. Hadjiev, D.E. Fan, D. Wang, L. Yu, S. Chen, Z. Ren, *Mater. Today Phys.* 2022, **27**, 100841.
127. R. Hu, F. Liu, H. Qiu, H. Miao, Q. Wang, H. Zhang, F. Wang, J. Yuan, *Processes.* 2022, **10**.
128. Y. Liu, Z. Song, Z. Li, M. Han, Y. Cheng, Z. Zheng, *Catal. Commun.* 2022, **164**, 106425.
129. Y. Wu, Z. Tian, S. Yuan, Z. Qi, Y. Feng, Y. Wang, R. Huang, Y. Zhao, J. Sun, W. Zhao, W. Guo, J. Feng, J. Sun, *Chem. Eng. J.* 2021, **411**, 128538.
130. L. Yu, L. Wu, B. McElhenny, S. Song, D. Luo, F. Zhang, Y. Yu, S. Chen, Z. Ren, *Energ. Environ. Sci.* 2020, **13**, 3439.
131. L. Wu, L. Yu, B. McElhenny, X. Xing, D. Luo, F. Zhang, J. Bao, S. Chen, Z. Ren, *Appl. Catal. B.* 2021, **94**, 120256.
132. W. Hao, C. Fu, Y. Wang, K. Yin, H. Yang, R. Yang, Z. Chen, *J. Energy Chem.* 2022, **75**, 26.
133. X. Sun, P. Yang, S. Wang, J. Hu, P. Chen, H. Xing, W. Zhu, *Int. J. Hydrogen Energy.* 2022, **47**, 28495.
134. Q. Lv, J. Han, X. Tan, W. Wang, L. Cao, B. Dong, *ACS Appl. Energy. Mater.* 2019, **2**, 3910.